

# A systematic study of the advection-dominated accretion flow for the origin of the X-ray emission in weakly magnetized low-level accreting neutron stars

Erlin Qiao<sup>1,2★</sup> and B.F. Liu<sup>1,2</sup>

<sup>1</sup>Key Laboratory of Space Astronomy and Technology, National Astronomical Observatories, Chinese Academy of Sciences, Beijing 100012, China

<sup>2</sup>School of Astronomy and Space Sciences, University of Chinese Academy of Sciences, 19A Yuquan Road, Beijing 100049, China

Accepted XXX. Received YYY; in original form ZZZ

## ABSTRACT

Observationally, the X-ray spectrum (0.5 – 10 keV) of low-level accreting neutron stars (NSs) ( $L_{0.5-10\text{keV}} \lesssim 10^{36} \text{ erg s}^{-1}$ ) can generally be well fitted by the model with two components, i.e., a thermal soft X-ray component plus a power-law component. Meanwhile, the fractional contribution of the power-law luminosity  $\eta$  ( $\eta \equiv L_{0.5-10\text{keV}}^{\text{power law}}/L_{0.5-10\text{keV}}$ ) varies with the X-ray luminosity  $L_{0.5-10\text{keV}}$ . In this paper, we systematically investigate the origin of such X-ray emission within the framework of the advection-dominated accretion flow (ADAF) around a weakly magnetized NS, in which the thermal soft X-ray component arises from the surface of the NS and the power-law component arises from the ADAF itself. We test the effects of the viscosity parameter  $\alpha$  in the ADAF and thermalized parameter  $f_{\text{th}}$  (describing the fraction of the ADAF energy released at the surface of the NS as thermal emission) on the relation of  $\eta$  versus  $L_{0.5-10\text{keV}}$ . It is found that  $\eta$  is nearly a constant ( $\sim$  zero) with  $L_{0.5-10\text{keV}}$  for different  $\alpha$  with  $f_{\text{th}} = 1$ , which is inconsistent with observations. Meanwhile, it is found that a change of  $f_{\text{th}}$  can significantly change the relation of  $\eta$  versus  $L_{0.5-10\text{keV}}$ . By comparing with a sample of non-pulsating NS-low mass X-ray binaries probably dominated by low-level accretion onto NSs, it is found that a small value of  $f_{\text{th}} \lesssim 0.1$  is needed to match the observed range of  $\eta \gtrsim 10\%$  in the diagram of  $\eta$  versus  $L_{0.5-10\text{keV}}$ . Finally, we argue that the small value of  $f_{\text{th}} \lesssim 0.1$  implies that the radiative efficiency of NSs with an ADAF accretion may not be as high as the predicted result previously of  $\epsilon \sim \frac{MG\dot{M}}{R_c \dot{M} c^2} \sim 0.2$  despite the existence of the hard surface.

**Key words:** accretion, accretion discs – stars: neutron – X-rays: binaries – black hole physics

## 1 INTRODUCTION

Most of the neutron star low-mass X-ray binaries (NS-LMXBs) are soft X-ray transients, which spend most of their time in the quiescent state, and are generally discovered when they first go into outburst (Campana et al. 1998, for review). NS-LMXBs can be divided into two distinct classes, i.e., the atoll-type NSs and the Z-type NSs, with the name derived from the shape they trace in the color-color diagram during the outburst and decay (Hasinger & van der Klis 1989). Atoll-type NSs are seen in the luminosity range from  $\lesssim 10^{-3} L_{\text{Edd}}$  up to  $\sim L_{\text{Edd}}$  (with  $L_{\text{Edd}} = 1.26 \times 10^{38} M/M_{\odot} \text{ erg s}^{-1}$ ), showing two distinct states, i.e., the soft state with a relatively higher mass accretion rate and the hard state with a relatively lower mass accretion rate as in black hole (BH) X-ray binaries according to the spectral and timing features. Z-type NSs accrete at or near the Eddington accretion rate with the

luminosity greater than  $\sim 0.5 L_{\text{Edd}}$  (e.g. Done & Gierliński 2003). The non-pulsating NS-LMXBs generally have a low magnetic field ( $B \lesssim 10^{8-9} \text{ G}$ ), so it is expected that the magnetic field does not affect the dynamics of the accretion flow. When the atoll-type NSs are in the soft state, the accretion is believed to be dominated by the optically thick, geometrically thin, cool disc (Shakura & Sunyaev 1973). Theoretically, in the case of Newtonian mechanics, one half of the gravitational energy will be released in the disc as the multi-color blackbody spectrum with a typical temperature  $\sim 10^7 \text{ K}$ , and the other half of the gravitational energy will be released in a thin boundary layer between the accretion disc and the surface of the NS (Popham & Narayan 1992; Inogamov & Sunyaev 1999; Popham & Sunyaev 2001; Frank et al. 2002). In the case of General Relativity, the energy released in the boundary layer is even larger, roughly twice than that of the disc (Syunyaev & Shakura 1986; Sibgatullin & Sunyaev 2000). The boundary layer is optically thick, and the temperature of the boundary layer is several times higher than that of the inner disc, producing a blackbody

★ E-mail: qiaoe@nao.cas.cn

spectrum with a higher temperature (Gilfanov & Sunyaev 2014, for review).

When the atoll-type NSs are in the hard state, theoretically, the accretion flow is suggested to be dominated by the so-called advection-dominated accretion flow (ADAF) (Narayan & Yi 1995; Esin et al. 1997). The properties of the ADAF around a NS are different from that of a BH due to the existence of a hard surface of NSs, which is critically examined by considering the effects of the boundary layer between the ADAF and the central NS (Medvedev & Narayan 2001; Medvedev 2004). Qiao & Liu (2018) investigated the properties of the ADAF around a weakly magnetized NS in the framework of the self-similar solution of the ADAF. In Qiao & Liu (2018), the authors assumed that a fraction,  $f_{\text{th}}$ , of the energy in the ADAF (including the internal energy and the radial kinetic energy) transferred onto the surface of the NS is thermalized at the surface of the NS as the soft photons to be scattered in the ADAF itself. Then the authors self-consistently calculate the structure of the ADAF and the corresponding emergent spectrum by considering the radiative coupling of the soft photons from the surface of the NS and the ADAF itself. Theoretically, it can be seen that if the authors take the viscosity parameter  $\alpha = 0.3$  and  $f_{\text{th}} = 1$ ,  $\sim 60\%$  of the gravitational energy will be released at the surface of the NS in the form of the blackbody emission (Qiao & Liu 2018).

Observationally, the X-ray spectrum of NS-LMXBs in the hard state has been well studied for the X-ray luminosity above  $\sim 10^{36}$  erg s $^{-1}$ . While for low-level accreting NSs, i.e., the X-ray luminosity below  $\sim 10^{36}$  erg s $^{-1}$ , especially the X-ray luminosity below  $\sim 10^{34}$  erg s $^{-1}$  (generally defined as the quiescent state), the X-ray spectrum is relatively less well understood (e.g. D'Angelo et al. 2015; Chakrabarty et al. 2014; Wijnands et al. 2015). The X-ray spectrum in the range of 0.5 – 10 keV for low-level accreting NSs can generally be well fitted with the model with two components, i.e., a thermal soft X-ray component plus a power-law component (e.g. Jonker et al. 2004b; Campana et al. 2008a,b; Fridriksson et al. 2010, 2011; Armas Padilla et al. 2013a; Degenaar et al. 2013; Campana et al. 2014; Parikh et al. 2017; Vats et al. 2018). For certain low-level accreting NSs, the temperature of the soft X-ray component decreases with decreasing the X-ray luminosity during the decay after the outburst (Armas Padilla et al. 2013b; Degenaar et al. 2013; Bahramian et al. 2014). Some studies show that the fractional contribution of the power-law luminosity  $\eta$  ( $\eta = L_{0.5-10\text{keV}}^{\text{power law}}/L_{0.5-10\text{keV}}$ ) is in a relatively narrow range of  $\eta \sim 40 - 60\%$  (Cackett et al. 2010; Fridriksson et al. 2011; Armas Padilla et al. 2013a; Campana et al. 2014; Homan et al. 2014; Bahramian et al. 2014). While some studies show that  $\eta$  can be in a wide range, e.g.,  $\eta$  is in the range of 10 – 40% for Aql X-1, Cen X-4 (Asai et al. 1996; Campana et al. 2000; Rutledge et al. 2000), 4U 2129+47 (Nowak et al. 2002), and even an extreme value of  $\eta \sim 100\%$  for SAX J1808.4-3658 (Campana et al. 2002). Jonker et al. (2004b) compiled a sample composed of 12 NS soft X-ray transients with the distance well-determined, the authors showed that there seems to be a positive correlation between  $\eta$  and  $L_{0.5-10\text{keV}}$  for  $L_{0.5-10\text{keV}} \gtrsim 2 \times 10^{33}$  erg s $^{-1}$ , below which there seems to be an anti-correlation between  $\eta$  and  $L_{0.5-10\text{keV}}$  for some sources.

So far, although a great of efforts have been made for investigating the X-ray spectrum in the range of 0.5-10 keV for low-level accreting NSs, the physical origin of the X-ray emission including both the thermal soft X-ray component and the power-law component, especially the relative strength between the thermal soft X-ray component and the power-law component is still under debate. Several models have been proposed for the origin

of the X-ray emission in the hard state and the quiescent state of NS-LMXBs. The thermal soft X-ray component could be from the crust cooling of the NS, which was heated during the last outburst (e.g. Brown et al. 1998; Campana et al. 2000; Rutledge et al. 1999, 2001a,b), or could be related to the low-level accretion onto the surface of the NS (e.g. Zampieri et al. 1995; Campana et al. 1997; Cackett et al. 2011; Bernardini et al. 2013; Qiao & Liu 2018). The power-law component could be related to the magnetic field of the NS, e.g., for SAX J1808.4-3658 (Campana et al. 2002), or also could be related to the low-level accretion onto the surface of the NS, e.g., for Cen X-4 (D'Angelo et al. 2015; Chakrabarty et al. 2014).

In this paper, we systematically investigate the origin of the X-ray emission in low-level accreting NSs within the framework of the self-similar solution of the ADAF as in Qiao & Liu (2018), in which the thermal soft X-ray component arises from the surface of the NS, and the power-law component arises from the ADAF itself. Additionally, in this paper, we update the calculation of Qiao & Liu (2018) with the effects of the NS spin considered. We consider that the internal energy and the radial kinetic energy of the ADAF as in Qiao & Liu (2018), as well as the rotational energy of the ADAF are transferred onto the surface of the NS. The rotational energy of the ADAF transferred onto the surface of the NS is dependent on the NS spin (Gilfanov & Sunyaev 2014). We assume that a fraction,  $f_{\text{th}}$ , of the total energy (including the internal energy, the radial kinetic energy and the rotational energy of the ADAF) transferred onto the surface of the NS is thermalized at the surface of the NS as the soft photons to be scattered in the ADAF. Then we self-consistently calculate the structure and the corresponding emergent spectrum of the ADAF by considering the radiative coupling between the soft photons from the surface of the NS and the ADAF itself. Based on the theoretical emergent spectra, we investigate the relation between  $\eta$  and  $L_{0.5-10\text{keV}}$ . Specifically, we test the effects of the viscosity parameter  $\alpha$  in the ADAF and the thermalized parameter  $f_{\text{th}}$  on the relation between  $\eta$  and  $L_{0.5-10\text{keV}}$ . It is found that the effect of  $\alpha$  on the relation between  $\eta$  and  $L_{0.5-10\text{keV}}$  is very little, and can nearly be neglected. As an example,  $\eta$  is nearly a constant ( $\sim$  zero) with  $L_{0.5-10\text{keV}}$  for different  $\alpha$  with  $f_{\text{th}} = 1$ . Meanwhile, we find that a change of  $f_{\text{th}}$  can significantly change the relation between  $\eta$  and  $L_{0.5-10\text{keV}}$ . By comparing with a sample of non-pulsating NS-LMXBs probably dominated by low-level accretion onto NSs, we find that a small value of  $f_{\text{th}} \lesssim 0.1$  can match the observed range of  $\eta \gtrsim 10\%$  in the diagram of  $\eta$  versus  $L_{0.5-10\text{keV}}$ . The derived small value of  $f_{\text{th}} \lesssim 0.1$  suggests that the radiative efficiency of a weakly magnetized NS with an ADAF accretion may not be as high as  $\epsilon \sim \frac{MGM}{R_*} / Mc^2 \sim 0.2$  as predicted previously. The model is briefly introduced in Section 2. The numerical results are shown in Section 3. The discussions are in Section 4 and the conclusions are in Section 5.

## 2 THE MODEL

We calculate the structure of the ADAF around a weakly magnetized NS within the framework of the self-similar solution of the ADAF as in Qiao & Liu (2018). In this paper, we consider that the internal energy and the radial kinetic energy of the ADAF as in Qiao & Liu (2018), as well as the rotational energy of the ADAF are transferred onto the surface of the NS. For clarity, we list the expression of the internal energy and the radial kinetic energy of the ADAF transferred onto the surface of the NS per second,  $L'_*$

(see also equation (9) in Qiao & Liu (2018)), which is as follows,

$$L'_* = 4\pi R_* H(R_*) |v(R_*)| \left[ U(R_*) + \frac{1}{2} \rho(R_*) v^2(R_*) \right], \quad (1)$$

where  $R_*$  is the radius of the NS, and  $U(R_*)$  is the internal energy of the gas at  $R_*$ ,  $H(R_*)$  is the scaleheight of the gas at  $R_*$ ,  $\rho(R_*)$  and  $v(R_*)$  are the density of the gas and the radial velocity of the gas at  $R_*$  respectively. The rotational energy of the ADAF transferred onto the surface of the NS per second,  $L_{\text{bl}}$ , ( $L_{\text{bl}}$  occurs actually in a thin boundary layer between the ADAF and the surface of the NS) can be expressed as,

$$L_{\text{bl}} = 2\pi^2 \dot{M} R_*^2 (\nu_* - \nu_{\text{NS}})^2, \quad (2)$$

where  $\nu_*$  is the rotational frequency of the accretion flow at  $R_*$  (with  $\nu_* = \Omega_*/2\pi$ , and  $\Omega_*$  being the angular velocity of the ADAF at  $R_*$ ), and  $\nu_{\text{NS}}$  is the rotational frequency of the NS. Then the total energy of the ADAF transferred onto the surface of the NS per second,  $L_*$ , can be expressed as the sum of  $L'_*$  and  $L_{\text{bl}}$ , i.e.,

$$L_* = L'_* + L_{\text{bl}}. \quad (3)$$

As in Qiao & Liu (2018), we assume that a fraction,  $f_{\text{th}}$ , of the energy,  $L_*$ , is thermalized at the surface of the NS as the soft photons to be scattered in the ADAF to self-consistently calculate the structure of the ADAF. In this case, if the radiation from the surface of the NS is isotropic, the effective temperature of the radiation  $T_*$  can then be given as,

$$T_* = \left( \frac{L_* f_{\text{th}}}{4\pi R_*^2 \sigma} \right)^{1/4}, \quad (4)$$

where  $\sigma$  is the Stefan-Boltzmann constant. Further, replacing equation (9) in Qiao & Liu (2018) by equation 3 in this paper, we can calculate the ion temperature  $T_i$ , electron temperature  $T_e$  and the advected fraction of the viscously dissipated energy  $f$  as in Qiao & Liu (2018) by specifying the model parameters, i.e., the NS mass  $m$  ( $m = M/M_\odot$ ), the NS radius  $R_*$ , the mass accretion rate  $\dot{m}^1$  (with  $\dot{m} = \dot{M}/\dot{M}_{\text{Edd}}$ ,  $\dot{M}_{\text{Edd}} = L_{\text{Edd}}/0.1c^2 = 1.39 \times 10^{18} M/M_\odot \text{ g s}^{-1}$ ), the viscosity parameter  $\alpha$ , the magnetic parameter  $\beta$  (with magnetic pressure  $p_m = B^2/8\pi = (1-\beta)p_{\text{tot}}$ ,  $p_{\text{tot}} = p_{\text{gas}} + p_m$ ),  $f_{\text{th}}$  describing the fraction of the total energy the ADAF transferred onto the surface of the NS to be thermalized as the blackbody emission, and the rotational frequency of the NS  $\nu_{\text{NS}}$ . The other quantities of ADAF, such as the Compton scattering optical depth in the vertical direction  $\tau_{\text{es}}$ , the Compton  $y$ -parameter (defined as  $y = \frac{4kT_e}{m_e c^2} \tau_{\text{es}}$ , with  $\tau_{\text{es}} < 1$ ), and the angular velocity  $\Omega$  of the ADAF can be calculated with the formulae derived by the self-similar solution of the ADAF accordingly [e.g., equation (4) in Qiao & Liu (2018)]. In this paper, we set the NS mass  $m = 1.4$ , and the NS radius  $R_* = 12.5 \text{ km}$  as in Qiao & Liu (2018). In the ADAF solution, the magnetic field is often relatively weak, as suggested by the magnetohydrodynamic simulations (Yuan & Narayan 2014, for review). Throughout this paper, we set  $\beta = 0.95$ . We test the effect of the rotational frequency of the NS  $\nu_{\text{NS}}$  on the structure of the ADAF in Section 4.1, it is found that the effect of  $\nu_{\text{NS}}$  on the structure of the ADAF can nearly be neglected. Throughout this paper, we set  $\nu_{\text{NS}} = 0$ . So, we have two parameters left, i.e.,  $\alpha$  and  $f_{\text{th}}$ . Finally, we calculate the emergent spectrum of the ADAF around a NS with the method of multi-scattering of soft photons in the hot gas (e.g. Manmoto et al. 1997; Qiao & Liu 2010, 2013, 2018).

<sup>1</sup> In this paper, a constant  $\dot{m}$  as a function of radius is assumed, which has been supported by the recent numerical simulations of the ADAF around a weakly magnetized NS (Bu et al. 2019).

### 3 THE RESULTS

#### 3.1 The effect of $\alpha$

In the panel (1) of Fig. 1, we plot the ratio of the energy transferred onto the surface of the NS per second  $L_*$  to the accretion luminosity  $L_G$  (defined as  $L_G = GM\dot{M}/R_*$ ),  $L_*/L_G$ , as a function of  $\dot{m}$  for different  $\alpha$  with  $f_{\text{th}} = 1.0$ . It can be seen that  $L_*/L_G$  increases very slightly with decreasing  $\dot{m}$  for  $\alpha = 0.1, 0.3, 0.6$  and  $1.0$  respectively. One can refer to Table 1 for the detailed numerical results<sup>2</sup>. Meanwhile, it is clear that, for a fixed  $\dot{m}$ , the derived  $L_*/L_G$  with a bigger value of  $\alpha$  is systematically higher than that of with a smaller value of  $\alpha$ , which can be understood as follows. Generally, as we know the luminosity of the ADAF around a BH can be expressed as  $L_{\text{ADAF}} \propto \dot{m}^2 \alpha^{-2}$  (e.g. Mahadevan 1997), so for a fixed  $\dot{m}$ , an increase the value of  $\alpha$  will result in a decrease of the radiation of the ADAF, which in turn means that the energy transferred into the event horizon of the BH will increase with increasing  $\alpha$ . As far as NSs, feedback exists between the energy transferred onto the surface of the NS and the ADAF itself. As a whole, due to the hot nature of the ADAF around both BHs and NSs, the radiation of the ADAF itself will decrease with increasing  $\alpha$ , which means that the energy transferred onto the surface of the NS will increase with increasing  $\alpha$  for a fixed  $\dot{m}$ , as can be seen in the panel (1) of Fig. 1. In the panel (2) of Fig. 1, we plot the temperature at the surface of the NS  $T_*$  as a function of  $\dot{m}$  for different  $\alpha$  with  $f_{\text{th}} = 1.0$ . It is clear that  $T_*$  decreases with decreasing  $\dot{m}$  for  $\alpha = 0.1, 0.3, 0.6$  and  $1.0$  respectively. Meanwhile, it can be seen that the effect of  $\alpha$  on the relation between  $T_*$  and  $\dot{m}$  is very little, which can be understood as, although roughly there is an increase of  $\sim 20\%$  for the value of  $L_*/L_G$  for taking  $\alpha = 1.0$  compared with taking  $\alpha = 0.1$  at a fixed  $\dot{m}$ , according to equation 4, the increase of  $T_*$  is only  $(1 + 20\%)^{1/4} - 1 \sim 4.7\%$ . One can refer to Table 1 for the detailed numerical results.

In order to more easily compare with observations, in the panel (3) of Fig. 1, we plot the corresponding fractional contribution of the power-law luminosity  $\eta$  as a function of the X-ray luminosity  $L_{0.5-10\text{keV}}$  for different  $\alpha$  with  $f_{\text{th}} = 1.0$ . It can be seen that  $\eta$  is nearly a constant ( $\sim$  zero) with  $L_{0.5-10\text{keV}}$  for all the value of  $\alpha$  as taking  $\alpha = 0.1, 0.3, 0.6$  and  $1.0$  respectively, which means that the X-ray spectrum in the range of  $0.5 - 10 \text{ keV}$  is completely dominated by the thermal component from the surface of the NS, and the contribution of the power-law component from the ADAF itself to the total X-ray luminosity  $L_{0.5-10\text{keV}}$  can nearly be neglected. One can refer to Table 1 for the detailed numerical results. Meanwhile, one can refer to the detailed emergent spectra in the panel (1) of Fig. 2 for  $\alpha = 0.1$  and  $f_{\text{th}} = 1.0$ , in the panel (2) of Fig. 2 for  $\alpha = 0.3$  and  $f_{\text{th}} = 1.0$ , in the panel (3) of Fig. 2 for  $\alpha = 0.6$  and  $f_{\text{th}} = 1.0$ , and in the panel (4) of Fig. 2 for  $\alpha = 1.0$  and  $f_{\text{th}} = 1.0$ . In order to more clearly show the effect of  $\alpha$  on the emergent spectra, in Fig. 3, we plot the emergent spectra for different  $\alpha$  with  $\dot{m} = 1 \times 10^{-3}$  and  $f_{\text{th}} = 1.0$ . As we expect, the relative contribution of the power-law luminosity from the ADAF itself to the thermal luminosity from the surface of the NS decreases with increasing with  $\alpha$ . However, we should also keep in mind that the X-ray spectrum in the range

<sup>2</sup> Since there is a critical mass accretion rate for the ADAF solution around a NS, i.e.,  $\dot{M}_{\text{crit}} \sim 0.1\alpha^2 \dot{M}_{\text{Edd}}$ , above which the ADAF solution cannot exist. As we can see,  $\dot{M}_{\text{crit}}$  is very sensitive to the viscosity parameter  $\alpha$ , so we roughly take  $\dot{m} = 1.0 \times 10^{-3}$  for  $\alpha = 0.1$ ,  $\dot{m} = 5.0 \times 10^{-3}$  for  $\alpha = 0.3$ ,  $\dot{m} = 1.5 \times 10^{-2}$  for  $\alpha = 0.6$ , and  $\dot{m} = 2.5 \times 10^{-3}$  for  $\alpha = 1.0$  as the upper limits of the mass accretion rate respectively in our calculations.



of 0.5 – 10 keV is completely dominated by the thermal component from the surface of the NS for all the value of  $\alpha$  as taking  $\alpha = 0.1, 0.3, 0.6$  and 1.0 respectively. In the panel (4) of Fig. 1, we plot the corresponding temperature at the surface of the NS  $T_*$  as a function of the X-ray luminosity  $L_{0.5-10\text{keV}}$  for different  $\alpha$  with  $f_{\text{th}} = 1.0$ . It is clear that  $T_*$  decreases with decreasing  $L_{0.5-10\text{keV}}$  for  $\alpha = 0.1, 0.3, 0.6$  and 1.0 respectively. One can also refer to Table 1 for the detailed numerical results.

### 3.2 The effect of $f_{\text{th}}$

In the panel (1) of Fig. 4, we plot  $L_*/L_G$  as a function of  $\dot{m}$  for different  $f_{\text{th}}$  with  $\alpha = 0.3$ . It can be seen that  $L_*/L_G$  increases slightly with decreasing  $\dot{m}$  for taking  $f_{\text{th}} = 1.0, 0.1, 0.05$  and 0.01 respectively. Meanwhile, as we can see that the effect of  $f_{\text{th}}$  on the relation between  $L_*/L_G$  and  $\dot{m}$  is very little. One can refer to Table 2 for the detailed numerical results. In the panel (2) of Fig. 4, we plot  $T_*$  as a function of  $\dot{m}$  for different  $f_{\text{th}}$  with  $\alpha = 0.3$ . It can be seen that  $T_*$  decreases with decreasing  $\dot{m}$  for  $f_{\text{th}} = 1.0, 0.1, 0.05$  and 0.01 respectively. Meanwhile, it is clear that, the value of  $T_*$  for a bigger  $f_{\text{th}}$  is systematically higher than that of for a smaller value of  $f_{\text{th}}$  for a fixed  $\dot{m}$ , as can be easily derived from equation 4 in this paper.

In order to more easily compare with observations, in the panel (3) of Fig. 4, we plot the corresponding fractional contribution of the power-law luminosity  $\eta$  as a function of the X-ray luminosity  $L_{0.5-10\text{keV}}$  for different  $f_{\text{th}}$  with  $\alpha = 0.3$ . It can be seen that, for  $f_{\text{th}} = 0.1$ ,  $\eta$  decreases from 6.1% to 3.9% for  $L_{0.5-10\text{keV}}$  decreasing from  $1.4 \times 10^{35}$  erg s<sup>-1</sup> to  $5.4 \times 10^{32}$  erg s<sup>-1</sup>, then  $\eta$  increases from 3.9% to 10.6% for  $L_{0.5-10\text{keV}}$  decreasing from  $5.4 \times 10^{32}$  erg s<sup>-1</sup> to  $2.8 \times 10^{30}$  erg s<sup>-1</sup>. A similar trend between  $\eta$  and  $L_{0.5-10\text{keV}}$  is shown for  $f_{\text{th}} = 0.05$  and  $f_{\text{th}} = 0.01$  respectively as for  $f_{\text{th}} = 0.1$ . (As a comparison,  $\eta$  versus  $L_{0.5-10\text{keV}}$  is also plotted for  $f_{\text{th}} = 1.0$ ). One can refer to Table 2 for the detailed numerical results. Meanwhile, one can refer to the detailed emergent spectra in the panel (1) of Fig. 5 for  $\alpha = 0.3$  and  $f_{\text{th}} = 1.0$ , in the panel (2) of Fig. 5 for  $\alpha = 0.3$  and  $f_{\text{th}} = 0.1$ , in the panel (3) of Fig. 5 for  $\alpha = 0.3$  and  $f_{\text{th}} = 0.05$ , and in the panel (4) of Fig. 5 for  $\alpha = 0.3$  and  $f_{\text{th}} = 0.01$ . In order to more clearly show the effect of  $f_{\text{th}}$  on the emergent spectra, we plot the emergent spectra for different  $f_{\text{th}}$  with  $\dot{m} = 5 \times 10^{-3}$  and  $\alpha = 0.3$  in Fig. 6. As we expect, both the temperature and luminosity of the thermal component decrease with decreasing  $f_{\text{th}}$ . As we can see from Fig. 6, the luminosity of the power-law component decreases with decreasing  $f_{\text{th}}$ , and the slope of the power-law component also decreases with decreasing  $f_{\text{th}}$ , which can be roughly understood as follows. As we know, in the NS case, the Compton cooling of the ADAF is dominated by the cooling of the seed photons from the surface of the NS, and the Compton cooling rate can be roughly expressed as,  $q_{\text{cmp}} = \frac{4kT_e}{m_e c^2} n_e \sigma_T c u \propto y c u / H$  (with  $k$  being the Boltzmann constant,  $T_e$  being the electron temperature,  $m_e$  being the electron mass,  $c$  being the speed of light,  $n_e$  being the electron number density,  $\sigma_T$  being the Thomson cross section,  $H$  being the scaleheight of the ADAF,  $y$  being the Compton  $y$ -parameter, and  $u$  being the energy density of the seed photons from the surface of the NS). With a decrease of  $f_{\text{th}}$  from  $f_{\text{th}} = 1.0$  to  $f_{\text{th}} = 0.01$ , the seed photon energy density  $u$  will decrease by a factor of  $\sim 100$ , and  $y$  will increase by a factor of only a few times [see

the panel (3) of Fig. 5 in Qiao & Liu (2018)]. Finally, there will be a few tens of the decrease of the power-law luminosity. As aforementioned, with a decrease of  $f_{\text{th}}$ ,  $y$  will increase, which will lead to a harder X-ray spectrum, i.e., the slope of the power-law component will decrease with decreasing  $f_{\text{th}}$ . In the panel (4) of Fig. 4, we plot the corresponding temperature at the surface of the NS  $T_*$  as a function of the X-ray luminosity  $L_{0.5-10\text{keV}}$  for different  $f_{\text{th}}$  with  $\alpha = 0.3$ . It is clear that  $T_*$  decreases with decreasing  $L_{0.5-10\text{keV}}$  for  $f_{\text{th}} = 1.0, 0.1, 0.05$  and 0.01 respectively, the trend of which is roughly consistent with observations. One can also refer to Table 2 for the detailed numerical results.

Here, we would like to argue that the effects of  $f_{\text{th}}$  on the relation between  $\eta$  and  $L_{0.5-10\text{keV}}$  can be understood as follows. As we can see from Fig. 6, for a fixed  $\dot{m}$ , although the power-law luminosity from the ADAF decreases with decreasing  $f_{\text{th}}$ , the thermal luminosity from the surface of the NS decreases more quickly, which actually means that the ratio of the power-law luminosity to the thermal luminosity increases with decreasing  $f_{\text{th}}$ . Specifically, if we focus on the energy range between 0.5 and 10 keV, for  $f_{\text{th}} = 0.01, 0.05, 0.1$  and 1.0,  $\eta$  is 39.2%, 12.5%, 6.1% and 0.1% respectively for  $\dot{m} = 5 \times 10^{-3}$ . For  $f_{\text{th}} = 0.01$ , if we increase the mass accretion rate as  $\dot{m} > 5 \times 10^{-3}$ , the ratio of the power-law luminosity to the thermal luminosity increases, and the value of  $\eta$  increases with increasing  $L_{0.5-10\text{keV}}$ , i.e., there is a positive correlation between  $\eta$  and  $L_{0.5-10\text{keV}}$ . However, we note that, for  $\dot{m} < 1 \times 10^{-3}$  corresponding  $L_{0.5-10\text{keV}} < 8.8 \times 10^{32}$  erg s<sup>-1</sup>, although the ratio of the power-law luminosity to the thermal luminosity decreases with decreasing  $\dot{m}$ , if we focus on the energy range between 0.5 and 10 keV,  $\eta$  increases with decreasing  $L_{0.5-10\text{keV}}$ , i.e., there is an anti-correlation between  $\eta$  and  $L_{0.5-10\text{keV}}$ . This is because, the temperature of the thermal component at the surface of the NS  $T_*$  decreases with decreasing  $\dot{m}$ , especially, for  $\dot{m} < 1 \times 10^{-3}$ , the peak emission of the thermal component from the surface of the NS moves out the range of 0.5 – 10keV. So although the ratio of the power-law luminosity to the thermal luminosity decreases with decreasing  $\dot{m}$ , if we focus on the energy range between 0.5 and 10 keV,  $\eta$  increases with decreasing  $\dot{m}$ . Meanwhile, because  $L_{0.5-10\text{keV}}$  decreases with decreasing  $\dot{m}$ ,  $\eta$  increases with decreasing  $L_{0.5-10\text{keV}}$ . For example, for  $\dot{m} = 1 \times 10^{-3}$ ,  $T_*$  is 0.098 keV, the peak emission is at  $T_{\text{max}} \approx 2.82T_* \approx 0.28$  keV (in  $L_\nu$  versus  $\nu$ ), a very minor fraction of the thermal component from the surface of the NS falls into the range of 0.5 – 10keV. The corresponding  $\eta$  is 40.5% and  $L_{0.5-10\text{keV}}$  is  $8.8 \times 10^{32}$  erg s<sup>-1</sup>. With the decrease of  $\dot{m}$  further, it is clear that  $\eta$  increases with decreasing  $L_{0.5-10\text{keV}}$ .

As we can see from the panel (3) of Fig. 4,  $\eta$  as a function of  $L_{0.5-10\text{keV}}$  for a bigger value of  $f_{\text{th}} = 0.1$  is systematically lower than that of for  $f_{\text{th}} = 0.05$  and  $f_{\text{th}} = 0.01$ . Meanwhile,  $f_{\text{th}} = 0.1$ , there still exists a correlation between  $\eta$  and  $L_{0.5-10\text{keV}}$ , i.e., there is a positive correlation between  $\eta$  and  $L_{0.5-10\text{keV}}$  for  $L_{0.5-10\text{keV}} \gtrsim$  a few times of  $10^{33}$  erg s<sup>-1</sup>, below which is an anti-correlation between  $\eta$  and  $L_{0.5-10\text{keV}}$ . Compared with the case for  $f_{\text{th}} = 0.05$  and  $f_{\text{th}} = 0.01$ , the slope of both the positive correlation and the anti-correlation between  $\eta$  and  $L_{0.5-10\text{keV}}$  becomes flatter, indicating that the correlation between  $\eta$  and  $L_{0.5-10\text{keV}}$  becomes weaker. Further, if we take the maximum value of  $f_{\text{th}}$  as  $f_{\text{th}} = 1.0$ ,  $\eta$  is nearly a constant ( $\sim$  zero) with  $L_{0.5-10\text{keV}}$ , and there is no correlation between  $\eta$  and  $L_{0.5-10\text{keV}}$ .

Finally, we would like to mention that the relation of  $\eta$  as a function of  $L_{0.5-10\text{keV}}$  for  $f_{\text{th}} = 1.0, 0.1, 0.05$  and 0.01 with  $\alpha = 0.3$  will systematically shift rightwards for taking a bigger value of  $\alpha$ , and will systematically shift leftwards for taking a smaller value of  $\alpha$  respectively. This is because an increase (or a decrease) of  $\alpha$  will

<sup>3</sup> In this paper, we always describe the relation between  $\eta$  and  $L_{0.5-10\text{keV}}$  from a higher value of  $L_{0.5-10\text{keV}}$  to a lower value of  $L_{0.5-10\text{keV}}$ . This is because the quiescent spectrum is often observed after the outburst as the order that the X-ray luminosity decreases with time.

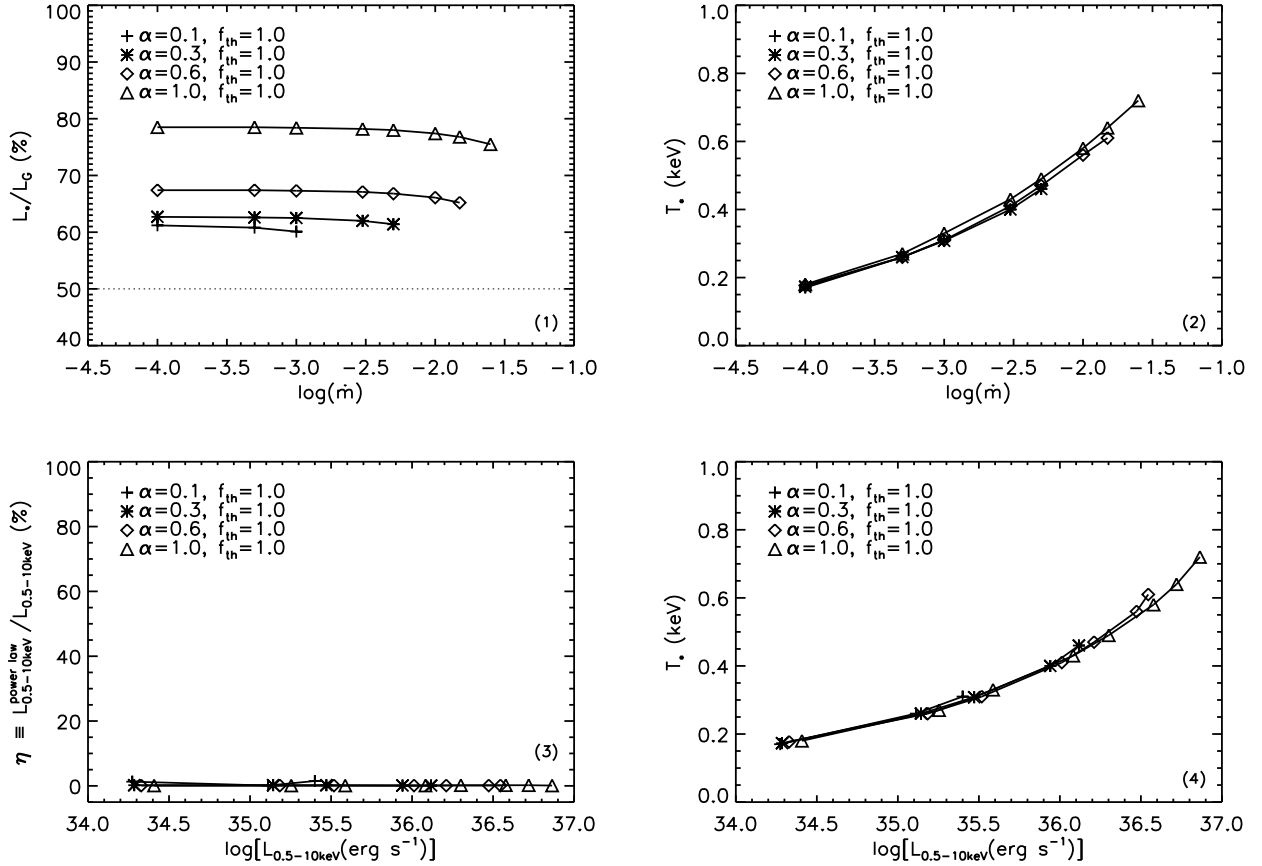


**Figure 1.** Panel (1): Ratio of the energy transferred onto the surface of the NS per second  $L_*$  to the accretion luminosity  $L_G$ ,  $L_*/L_G$ , as a function of  $\dot{m}$ . Panel (2): Effective temperature at the surface of the NS  $T_*$  as a function of  $\dot{m}$ . Panel (3): Fractional contribution of the power-law luminosity  $\eta \equiv L_{0.5-10\text{keV}}^{\text{power law}} / L_{0.5-10\text{keV}}$  as a function of the X-ray luminosity  $L_{0.5-10\text{keV}}$ . Panel (4): Effective temperature at the surface of the NS  $T_*$  as a function of the X-ray luminosity  $L_{0.5-10\text{keV}}$ .

only lead to an increase (or a decrease) of the upper limit of the X-ray luminosity but will not systematically change the trend of the shape of the X-ray spectrum with the X-ray luminosity.

### 3.3 Comparison with observations for $\eta$ versus

$L_{0.5-10\text{keV}}$ —the effect of  $f_{th}$

As has been shown in Section 3.1 and Section 3.2, we test the effect of the viscosity parameter  $\alpha$ , and  $f_{th}$  describing the fraction of the total energy of the ADAF transferred onto the surface of the NS to be thermalized as the thermal emission on the relation between  $\eta$  and  $L_{0.5-10\text{keV}}$  respectively. It is found that, theoretically, the effect of  $\alpha$  on the relation between  $\eta$  and  $L_{0.5-10\text{keV}}$  is very little, and can nearly be neglected. Specifically,  $\eta$  is nearly a constant ( $\sim$  zero) with  $L_{0.5-10\text{keV}}$  for different  $\alpha$  with  $f_{th} = 1$ , which is inconsistent with observations. So in this paper, we focus on the effect of  $f_{th}$  on the relation between  $\eta$  and  $L_{0.5-10\text{keV}}$ , and compare the theoretical results with observations.

We collect the observational data of  $\eta$  versus  $L_{0.5-10\text{keV}}$  from literatures for the sources probably dominated by low-level accretion onto NSs. Specifically, we collect a sample composed of 16 non-pulsating NS-LMXBs with the measurements of  $\eta$  and  $L_{0.5-10\text{keV}}$ , i.e., Cen X-4 (Asai et al. 1996; Cackett et al. 2010, 2013), Aql X-1 (Rutledge et al. 2002; Campana et al. 2014), MXB 1659-29 (Wijnands et al. 2004), XTE J1709-

267 (Jonker et al. 2004b), KS 1731-260 (Wijnands et al. 2001), SAX J1810.8-2609 (Jonker et al. 2004a; Allen et al. 2018), XTE J2123-058 (Tomsick et al. 2004), 4U 1608-52 (Asai et al. 1996), EXO 1745-248 (Wijnands et al. 2005; Rivera Sandoval et al. 2018), AX J1754.2-2754, IRXS J171824.2-402934 and IRXH J173523.7-354013 (Armas Padilla et al. 2013a), XTE J1701-462 (Fridriksson et al. 2011), Terzan 5 X-3 (Swift J174805.3-244637) (Bahramian et al. 2014), EXO 0748-676 (Degenaar et al. 2009; Zhang et al. 2011), and GRS 1747-312 (Vats et al. 2018). Meanwhile, we also include a typical accreting millisecond X-ray pulsar (AMXP) SAX J1808.4-3658 for comparison (Campana et al. 2002; Heinke et al. 2007, 2009). Some comments for the data are as follows. KS 1731-260 and MXB 1659-29 are two quasi-persistent sources. The thermal soft X-ray component of the X-ray spectrum of KS 1731-260 and MXB 1659-29 has been explained as the emission of the crust cooling (Wijnands et al. 2017, for review). However, the origin of the power-law component of the X-ray spectrum is unclear, which is very probably related with the low-level accretion onto NSs. Here as a comparison, we still put the data of KS 1731-260 and MXB 1659-29 in the present paper. One can refer to Fig. 7 for all the data in detail.

As we can see in Fig. 7, for nearly all the data, the value of  $\eta$  is greater than  $\sim 10\%$ . Meanwhile, it seems that systematically there is a positive correlation between  $\eta$  and  $L_{0.5-10\text{keV}}$  for  $L_{0.5-10\text{keV}} \gtrsim 2 \times 10^{33} \text{ erg s}^{-1}$ , below which there is an anti-

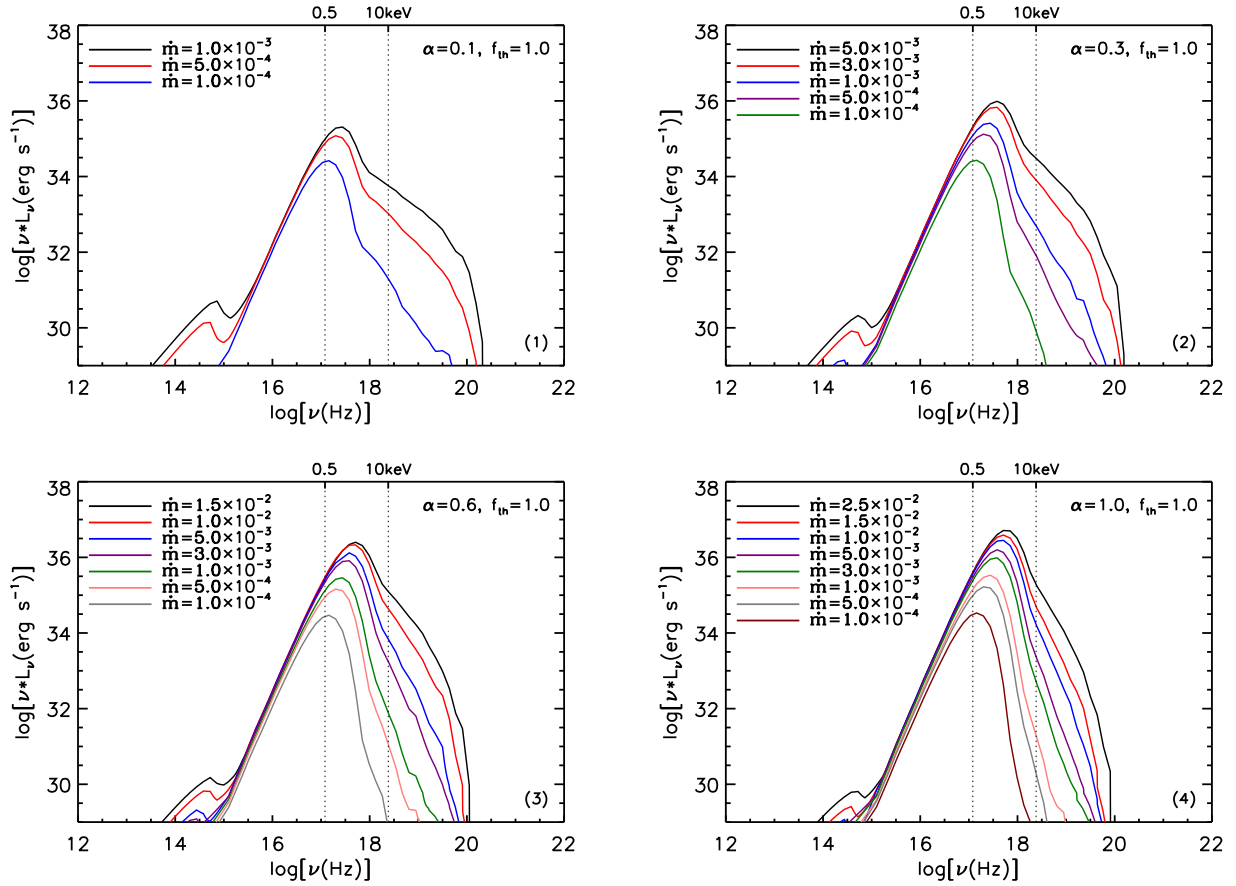


**Figure 2.** Panel (1): Emergent spectra of the ADAF around a NS for  $\alpha = 0.1$  and  $f_{\text{th}} = 1.0$ . Panel (2): Emergent spectra of the ADAF around a NS for  $\alpha = 0.3$  and  $f_{\text{th}} = 1.0$ . Panel (3): Emergent spectra of the ADAF around a NS for  $\alpha = 0.6$  and  $f_{\text{th}} = 1.0$ . Panel (4): Emergent spectra of the ADAF around a NS for  $\alpha = 1.0$  and  $f_{\text{th}} = 1.0$ .

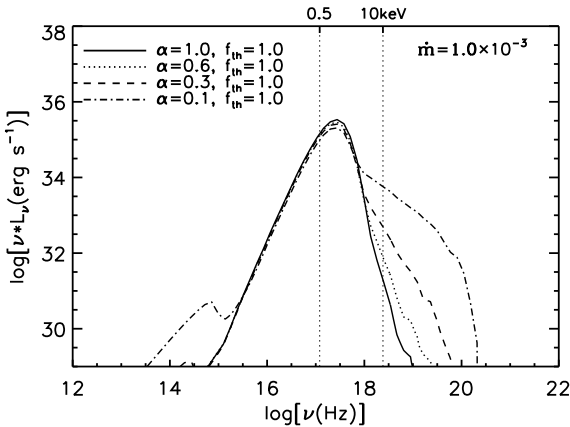


**Figure 3.** Emergent spectra of the ADAF around a NS for different  $\alpha$  with  $f_{\text{th}} = 1.0$  and  $\dot{m} = 1 \times 10^{-3}$ .

correlation between  $\eta$  and  $L_{0.5-10\text{keV}}$  for some sources (see also in Fig. 5 of Jonker et al. (2004b)). The positive correlation between  $\eta$  and  $L_{0.5-10\text{keV}}$  is dominated by the observational data of XTE J1709-267, in which  $\eta$  decreases from 72% to less than 19% for  $L_{0.5-10\text{keV}}$  decreasing from  $\sim 5 \times 10^{34}$  to  $2 \times 10^{33}$  erg s $^{-1}$

(Jonker et al. 2004b). A possible anti-correlation between  $\eta$  and  $L_{0.5-10\text{keV}}$  is observed in MXB 1659-29 in the range of  $L_{0.5-10\text{keV}} \sim 3 \times 10^{32} - 3 \times 10^{33}$  erg s $^{-1}$  (Wijnands et al. 2004), and in KS 1731-260 in the range of  $L_{0.5-10\text{keV}} \sim 2 \times 10^{32} - 2 \times 10^{33}$  erg s $^{-1}$  (Wijnands et al. 2001). However, we should keep in mind that, the derived value of  $\eta$  for MXB 1659-29 and KS 1731-260 are only upper limits, the anti-correlation between  $\eta$  and  $L_{0.5-10\text{keV}}$  is still to be confirmed by the observations in the future.

In Fig. 7, we plot the theoretical results of  $\eta$  as a function of  $L_{0.5-10\text{keV}}$  for different  $f_{\text{th}}$  with  $\alpha = 0.3$  as a comparison. The solid line is for  $f_{\text{th}} = 1$ , the dotted line is for  $f_{\text{th}} = 0.1$ , the dashed line is for  $f_{\text{th}} = 0.05$ , and the dot-dashed line is for  $f_{\text{th}} = 0.01$ . It is clear that, for nearly all the observational data, the value of  $\eta$  is  $\gtrsim 10\%$ , which requires  $f_{\text{th}} \lesssim 0.1$ . As for EXO 1745-248, besides the data in (Wijnands et al. 2005), the new observational data also show that the X-ray spectrum is nearly completely dominated by a power-law component in the range of  $L_{0.5-10\text{keV}} \sim 10^{32} - 10^{34}$  erg s $^{-1}$ , indicating an extreme value of  $\eta \sim 100\%$  (only at the highest quiescent X-ray luminosity of  $L_{0.5-10\text{keV}} \sim 10^{34}$  erg s $^{-1}$ , an additional thermal soft X-ray component is needed to improve the spectral fitting), the origin of which is still not well understood (Rivera Sandoval et al. 2018). If the power-law X-ray emission in EXO 1745-248 can be explained in the framework of our ADAF model, which means that  $f_{\text{th}}$  must be an extreme low value of  $f_{\text{th}} \sim 0$ . SAX J1808.4-3658 is an AMXP, which could have a sizeable magnetic field (gener-

**Table 1.** Radiative features of the ADAF around NSs for different  $\dot{m}$  with  $\alpha = 0.1, 0.3, 0.6$  and  $1.0$  respectively.  $L_*/L_G$  is the ratio of the energy of the ADAF transferred onto the surface of the NS per second to the accretion luminosity.  $T_*$  is the effective temperature at the surface of the NS.  $L_{0.5-10\text{keV}}^{\text{power law}}/L_{0.5-10\text{keV}}$  is the fractional contribution of the power-law luminosity.  $L_{0.5-10\text{keV}}$  is the luminosity between 0.5 and 10 keV.

$m = 1.4, R_* = 12.5 \text{ km}, \beta = 0.95$ and $\nu_{\text{NS}} = 0 \text{ (Hz)}$						
$\alpha$	$f_{\text{th}}$	$\dot{m}$	$L_*/L_G$	$T_*$ (keV)	$\eta$ (%)	$L_{0.5-10\text{keV}}$ (erg s $^{-1}$ )
0.1	1.0	$1.0 \times 10^{-3}$	60.1%	0.31	1.5	$2.5 \times 10^{35}$
0.1	1.0	$5.0 \times 10^{-4}$	60.8%	0.26	0.1	$1.3 \times 10^{35}$
0.1	1.0	$1.0 \times 10^{-4}$	61.2%	0.17	1.3	$1.9 \times 10^{34}$
0.3	1.0	$5.0 \times 10^{-3}$	61.4%	0.46	0.1	$1.3 \times 10^{36}$
0.3	1.0	$3.0 \times 10^{-3}$	62.0%	0.40	0.1	$8.7 \times 10^{35}$
0.3	1.0	$1.0 \times 10^{-3}$	62.5%	0.31	0.2	$3.0 \times 10^{35}$
0.3	1.0	$5.0 \times 10^{-4}$	62.6%	0.26	0.2	$1.4 \times 10^{35}$
0.3	1.0	$1.0 \times 10^{-4}$	62.7%	0.17	0.2	$1.9 \times 10^{34}$
0.6	1.0	$1.5 \times 10^{-2}$	65.2%	0.61	0.1	$3.5 \times 10^{36}$
0.6	1.0	$1.0 \times 10^{-2}$	66.1%	0.56	0.1	$3.0 \times 10^{36}$
0.6	1.0	$5.0 \times 10^{-3}$	66.8%	0.47	0.1	$1.6 \times 10^{36}$
0.6	1.0	$3.0 \times 10^{-3}$	67.1%	0.41	0.1	$1.0 \times 10^{36}$
0.6	1.0	$1.0 \times 10^{-3}$	67.3%	0.31	0.1	$3.3 \times 10^{35}$
0.6	1.0	$5.0 \times 10^{-4}$	67.4%	0.26	0.1	$1.5 \times 10^{35}$
0.6	1.0	$1.0 \times 10^{-4}$	67.4%	0.18	0.1	$2.1 \times 10^{34}$
1.0	1.0	$2.5 \times 10^{-2}$	75.5%	0.72	0.1	$7.3 \times 10^{36}$
1.0	1.0	$1.5 \times 10^{-2}$	76.8%	0.64	0.2	$5.2 \times 10^{36}$
1.0	1.0	$1.0 \times 10^{-2}$	77.4%	0.58	0.2	$3.8 \times 10^{36}$
1.0	1.0	$5.0 \times 10^{-3}$	78.0%	0.49	0.2	$2.0 \times 10^{36}$
1.0	1.0	$3.0 \times 10^{-3}$	78.2%	0.43	0.1	$1.2 \times 10^{36}$
1.0	1.0	$1.0 \times 10^{-3}$	78.4%	0.33	0.1	$3.9 \times 10^{35}$
1.0	1.0	$5.0 \times 10^{-4}$	78.5%	0.27	0.1	$1.8 \times 10^{35}$
1.0	1.0	$1.0 \times 10^{-4}$	78.5%	0.18	0.1	$2.6 \times 10^{34}$

ally  $\sim 10^{8-9}$ G). The quiescent spectrum of SAX J1808.4-3658 is completely dominated by a power-law component, the origin of which thus is probably related to the magnetic field (e.g. Stella et al. 1994; Burderi et al. 2003; Campana et al. 2002). However, in the present paper SAX J1808.4-3658 is still included as in Fig. 7. This is because observationally the effect of the magnetic field on the X-ray spectrum of AMXPs is still under debate (e.g. Wijnands et al. 2015). Actually, it is poorly understood why some NS-LMXBs show pulsations and others do not, and it is not proven that this is due to a difference in magnetic field strength. For instance, Aql X-1 is such a source with only the intermittent millisecond X-ray pulsations observed (Casella et al. 2008; Qiao & Liu 2019). Again, if the power-law emission in SAX J1808.4-3658 can be explained with the ADAF model around a NS, which means that an extreme value of  $f_{\text{th}} \sim 0$  is required.

In addition, as we can see in Fig. 7, our model intrinsically predicts a positive correlation between  $\eta$  and  $L_{0.5-10\text{keV}}$  for  $L_{0.5-10\text{keV}} \gtrsim$  a few times of  $10^{33}$  erg s $^{-1}$ , and an anti-correlation between  $\eta$  and  $L_{0.5-10\text{keV}}$  for  $L_{0.5-10\text{keV}} \lesssim$  a few times of  $10^{33}$  erg s $^{-1}$  for taking a relatively lower value of  $f_{\text{th}} = 0.1, 0.05$  and  $0.01$  respectively. As can be seen that, the slope of both the positive correlation and the anti-correlation between  $\eta$  and  $L_{0.5-10\text{keV}}$  can be significantly affected by the value of  $f_{\text{th}}$ , i.e. both the positive correlation and the anti-correlation between  $\eta$  and  $L_{0.5-10\text{keV}}$  become weaker with increasing  $f_{\text{th}}$ . Here we expect that the predicted correlation between  $\eta$  and  $L_{0.5-10\text{keV}}$  from our model could be confirmed by more accurate observations in the future although there are some observational clues of such correlations, e.g., the observations for XTE J1709-267, MXB 1659-29 and KS 1731-260. We should also keep

in mind that, as the first order approximation, currently, our theoretical results can only very roughly reproduce a trend of both the positive correlation and the anti-correlation. A more detailed calculation is still needed to more accurately explain the observations. For example, in this paper, we always assume that  $f_{\text{th}}$  is a constant for different  $\dot{m}$ . Actually, if we consider  $f_{\text{th}}$  as a function of  $\dot{m}$ , i.e.  $f_{\text{th}}(\dot{m})$ , definitely we can more flexibly fit the relation between  $\eta$  and  $L_{0.5-10\text{keV}}$ , which is beyond the scope of the present paper, and will be done in detail in the future work.

Finally, we would like to mention that in this paper, we set the NS mass  $m = 1.4$ , and the NS radius  $R_* = 12.5$  km as in Qiao & Liu (2018). Theoretically, a change of  $m$  and  $R_*$  can affect the relation of  $\eta$  versus  $L_{0.5-10\text{keV}}$  to some extent. However, observationally the value of  $m$  and  $R_*$  can be restricted in a very narrow range, i.e.,  $m \sim 1.4 - 2.0$  and  $R_* \sim 10$  km. (e.g. Degenaar & Suleimanov 2018, for review). So a change of  $m$  and  $R_*$  in a reasonable range will not change our main conclusions. Meanwhile, as we know, when the LMXBs are in the hard state or the quiescent state, it is generally suggested that the accretion flow exists in the form of a two-component structure with an inner ADAF plus an outer truncated thin disc, and the contribution of the truncated disc to the total emission depends on the truncation radius of the disc. The relative contribution of the truncated disc to the total emission increases with increasing the mass accretion rate as generally the truncation radius decreases with increasing the mass accretion rate. In particular, if the truncation radius is less than  $\sim 10R_S$  (with  $R_S$  being the Schwarzschild radius, and  $R_S = 2.95 \times 10^5$  m cm), it is expected that the truncated disc can contribute a significant fraction of the thermal soft X-ray emission. However, theoretically



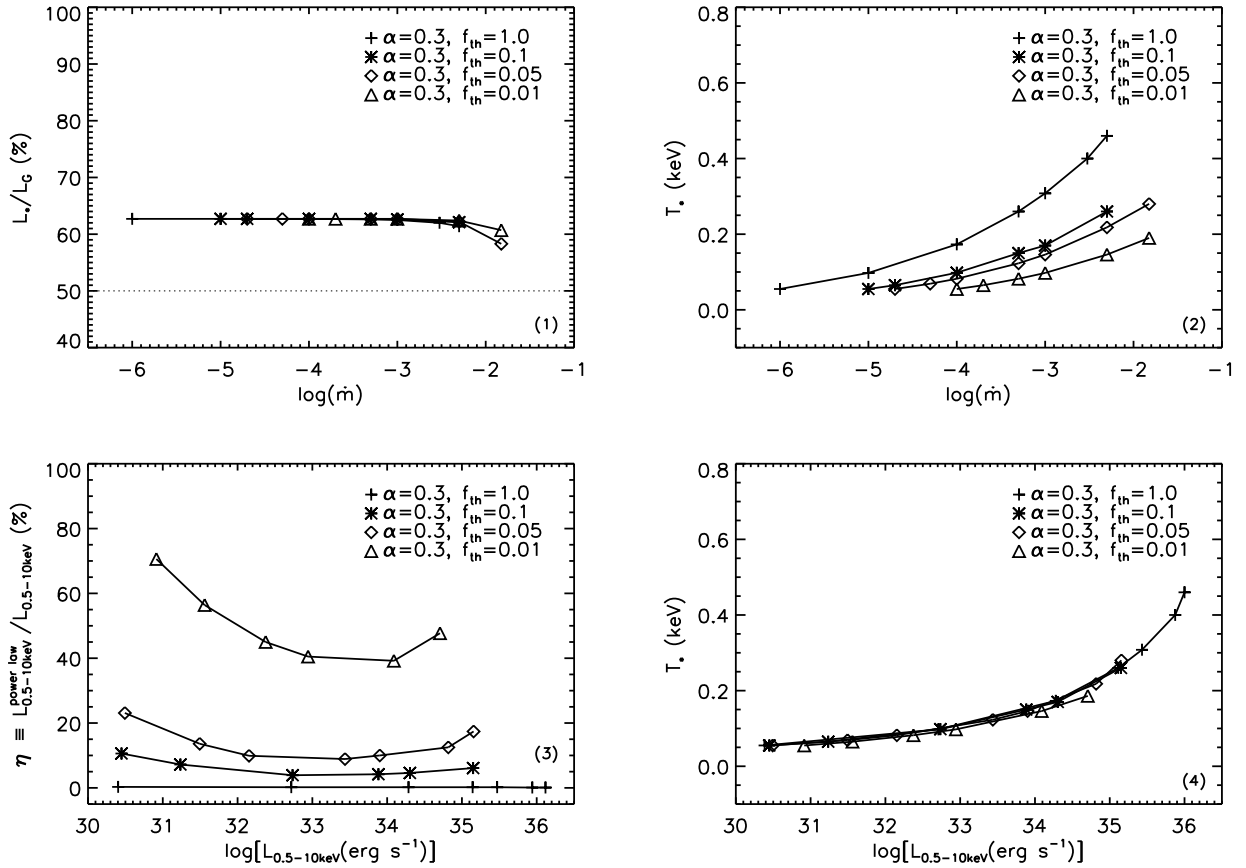


**Figure 4.** Panel (1): Ratio of the energy transferred onto the surface of the NS per second  $L_*$  to the accretion luminosity  $L_G$ ,  $L_*/L_G$ , as a function of  $\dot{m}$ . Panel (2): Effective temperature at the surface of the NS  $T_*$  as a function of  $\dot{m}$ . Panel (3): Fractional contribution of the power-law luminosity  $\eta \equiv L_{0.5-10\text{keV}}^{\text{power law}}/L_{0.5-10\text{keV}}$  as a function of the X-ray luminosity  $L_{0.5-10\text{keV}}$ . Panel (4): Effective temperature at the surface of the NS  $T_*$  as a function of the X-ray luminosity  $L_{0.5-10\text{keV}}$ .

only very fewer models can predict the value of the truncation radius for a given mass accretion rate. Here for example, the value of the truncation radius as a function of mass accretion rate has been proposed around a BH within the framework of the disc evaporation model (e.g. Liu et al. 1999; Meyer et al. 2000a,b; Qiao & Liu 2009, 2010; Qiao et al. 2013; Taam et al. 2012). Specifically, in Taam et al. (2012), a formula for the truncation radius  $r_{\text{tr}}$  (in units of  $R_S$ ) as functions of  $\dot{m}$ , the viscosity parameter  $\alpha$  and the magnetic parameter  $\beta$  is given, which is as follows,

$$r_{\text{tr}} \approx 17.3 \dot{m}^{-0.886} \alpha^{0.07} \beta^{4.61}. \quad (5)$$

It is clear that  $r_{\text{tr}}$  is very weakly dependent on  $\alpha$ , while is very strongly dependent on  $\beta$ . For example, if we take  $\alpha = 0.3$ ,  $\beta = 0.95$  for a weaker magnetic field as expected in ADAF, and  $\dot{m} = 5 \times 10^{-3}$  (the upper limit that the ADAF solution can exist for  $\alpha = 0.3$ ), the truncation radius  $r_{\text{tr}}$  is  $\sim 1370$ , the contribution of which in soft X-ray emission can definitely be neglected. Here in the present paper as the first step we simply neglect the contribution of the truncated disc to the thermal soft X-ray emission and further to the value of  $\eta$  if indeed the disc evaporation model works for the truncation of the accretion disc in NS-LMXBs.

## 4 DISCUSSIONS

### 4.1 The effect of the NS spin

In this paper, we calculate the structure and the corresponding emergent spectrum of the ADAF around a weakly magnetized NS within the framework of the self-similar solution of the ADAF as in Qiao & Liu (2018). Additionally, we consider the effect of the spin of the NS on the structure of the ADAF, which was not considered in Qiao & Liu (2018). In the panel (1) of Fig. 8, we plot the ion temperature  $T_i$  and the electron temperature  $T_e$  of the ADAF as a function of the radius  $R/R_S$  for different rotational frequency  $\nu_{\text{NS}}$  as taking  $\nu_{\text{NS}} = 0, 200, 500$  and  $700$  Hz respectively with  $\dot{m} = 5 \times 10^{-3}$ . In the calculation, we fix  $\alpha = 0.3$  and  $f_{\text{th}} = 1.0$ . In the panel (2) of Fig. 8, we plot the Compton scattering optical depth  $\tau_{\text{es}}$  in the vertical direction of the ADAF as a function of  $R/R_S$  for different  $\nu_{\text{NS}}$  as taking  $\nu_{\text{NS}} = 0, 200, 500$  and  $700$  Hz respectively with  $\dot{m} = 5 \times 10^{-3}$ . In the panel (3) of Fig. 8, we plot the Compton  $y$ -parameter of the ADAF as a function of  $R/R_S$  for different  $\nu_{\text{NS}}$  as taking  $\nu_{\text{NS}} = 0, 200, 500$  and  $700$  Hz respectively with  $\dot{m} = 5 \times 10^{-3}$ . In the panel (4) of Fig. 8, we plot the ratio of the angular velocity of the ADAF to the Keplerian angular velocity,  $\Omega/\Omega_K$  (with  $\Omega_K$  being the Keplerian angular velocity), as a function of  $R/R_S$  for different  $\nu_{\text{NS}}$  as taking  $\nu_{\text{NS}} = 0, 200, 500$  and  $700$  Hz respectively with  $\dot{m} = 5 \times 10^{-3}$ . It can be seen that the effects of  $\nu_{\text{NS}}$  on  $T_i$ ,  $T_e$ ,  $\tau_{\text{es}}$ ,  $y$  and  $\Omega/\Omega_K$  of the ADAF are very little, and can nearly be ne-



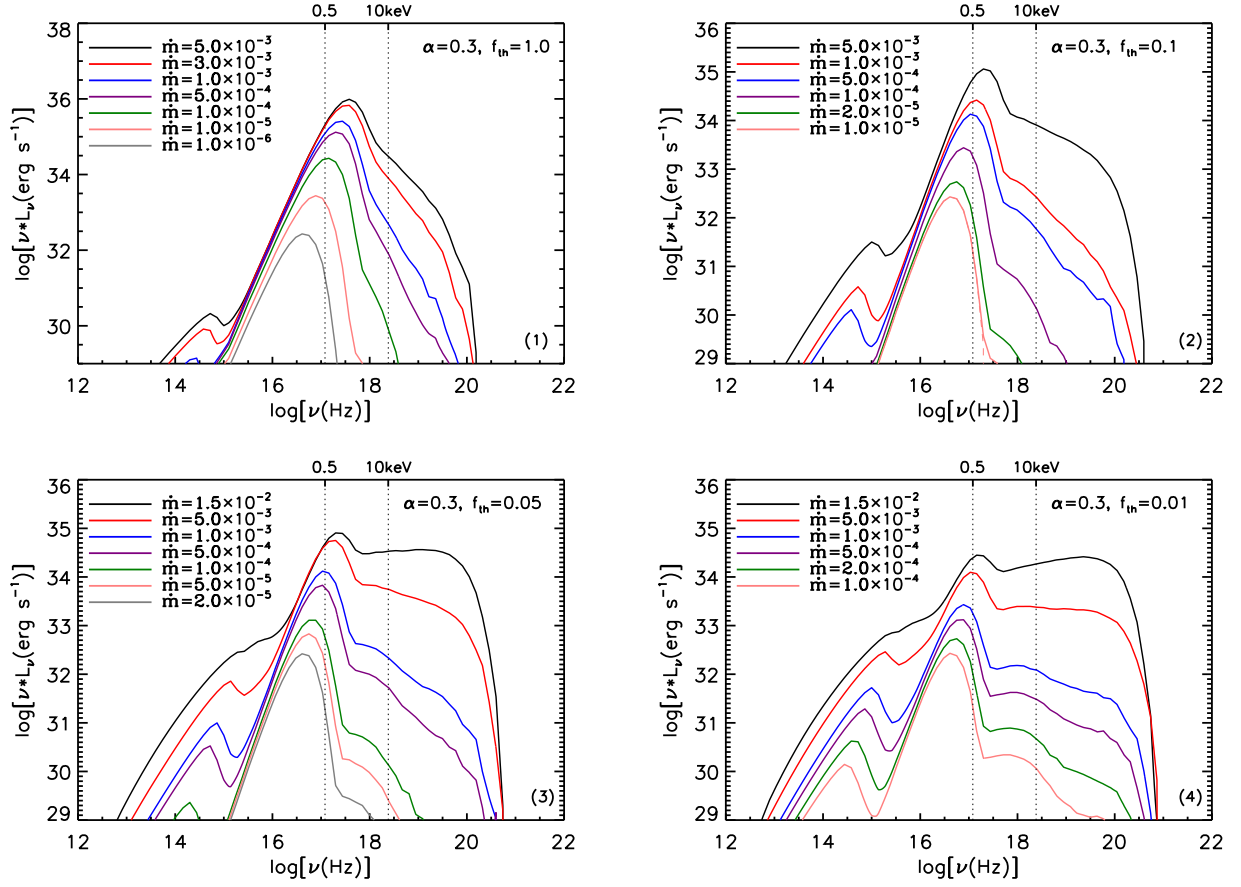


**Figure 5.** Panel (1): Emergent spectra of the ADAF around a NS for  $\alpha = 0.3$  and  $f_{\text{th}} = 1.0$ . Panel (2): Emergent spectra of the ADAF around a NS for  $\alpha = 0.3$  and  $f_{\text{th}} = 0.1$ . Panel (3): Emergent spectra of the ADAF around a NS for  $\alpha = 0.3$  and  $f_{\text{th}} = 0.05$ . Panel (4): Emergent spectra of the ADAF around a NS for  $\alpha = 0.3$  and  $f_{\text{th}} = 0.01$ .

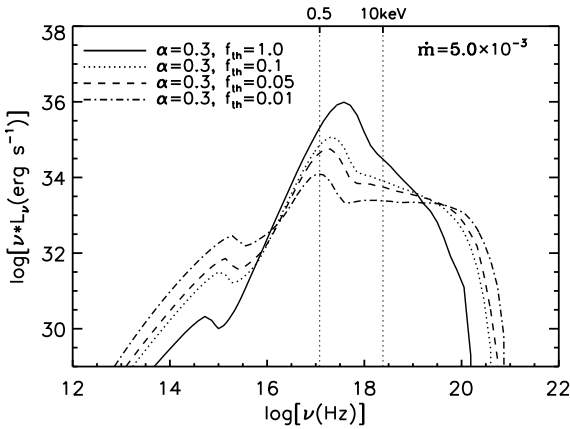


**Figure 6.** Emergent spectra of the ADAF around a NS for different  $f_{\text{th}}$  with  $\alpha = 0.3$  and  $\dot{m} = 5 \times 10^{-3}$ .

glected. This is because, in this paper as in equation 2 of Section 2, the effect of  $v_{\text{NS}}$  is mainly reflected as the contribution of the soft photons to be scattered in the ADAF. However, the ADAF solution is hot, the energy of the ADAF transferred onto the surface of the NS is always dominated by the internal energy and the radial ki-

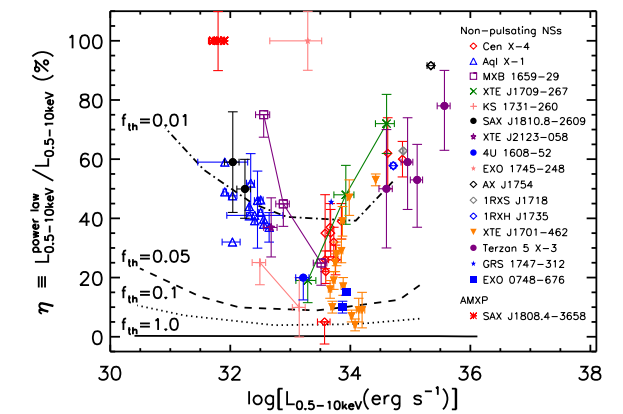


**Figure 7.** The fractional contribution of the power-law luminosity  $\eta$  versus the X-ray luminosity  $L_{0.5-10\text{keV}}$ . The solid line, the dotted line, the dashed line, and the dot-dashed lines refer to the theoretical results for taking  $f_{\text{th}} = 1.0, 0.1, 0.05$  and  $0.01$  respectively. In the calculations,  $\alpha = 0.3$  is adopted. The coloured symbols are the observational data of 16 non-pulsating NS-LMXBs probably dominated by low-level accretion onto NSs. One AMXP SAX J1808.4-3658 is included for comparison. One can refer to Section 3.3 for the references for details.

**Table 2.** Radiative features of the ADAF around NSs for different  $\dot{m}$  with  $f_{\text{th}} = 1.0, 0.1, 0.05$  and  $0.01$  respectively.  $L_*/L_G$  is the ratio of the energy of the ADAF transferred onto the surface of the NS per second to the accretion luminosity.  $T_*$  is the effective temperature at the surface of the NS.  $L_{0.5-10\text{keV}}^{\text{power law}}/L_{0.5-10\text{keV}}$  is the fractional contribution of the power-law luminosity.  $L_{0.5-10\text{keV}}$  is the luminosity between 0.5 and 10 keV.

$m = 1.4, R_* = 12.5 \text{ km}, \beta = 0.95$ and $\nu_{\text{NS}} = 0 \text{ (Hz)}$						
$\alpha$	$f_{\text{th}}$	$\dot{m}$	$L_*/L_G$	$T_*$ (keV)	$\eta$ (%)	$L_{0.5-10\text{keV}}$ (erg s $^{-1}$ )
0.3	1.0	$5.0 \times 10^{-3}$	61.4%	0.46	0.1	$1.3 \times 10^{36}$
0.3	1.0	$3.0 \times 10^{-3}$	62.0%	0.40	0.1	$8.7 \times 10^{35}$
0.3	1.0	$1.0 \times 10^{-3}$	62.5%	0.31	0.2	$3.0 \times 10^{35}$
0.3	1.0	$5.0 \times 10^{-4}$	62.6%	0.26	0.2	$1.4 \times 10^{35}$
0.3	1.0	$1.0 \times 10^{-4}$	62.7%	0.17	0.2	$1.9 \times 10^{34}$
0.3	1.0	$1.0 \times 10^{-5}$	62.7%	0.098	0.2	$5.2 \times 10^{32}$
0.3	1.0	$1.0 \times 10^{-6}$	62.7%	0.055	0.3	$2.5 \times 10^{30}$
0.3	0.1	$5.0 \times 10^{-3}$	62.1%	0.26	6.1	$1.4 \times 10^{35}$
0.3	0.1	$1.0 \times 10^{-3}$	62.6%	0.17	4.5	$2.0 \times 10^{34}$
0.3	0.1	$5.0 \times 10^{-4}$	62.7%	0.15	4.2	$7.6 \times 10^{33}$
0.3	0.1	$1.0 \times 10^{-4}$	62.7%	0.098	3.9	$5.4 \times 10^{32}$
0.3	0.1	$2.0 \times 10^{-5}$	62.7%	0.065	7.2	$1.7 \times 10^{31}$
0.3	0.1	$1.0 \times 10^{-5}$	62.7%	0.055	10.6	$2.8 \times 10^{30}$
0.3	0.05	$1.5 \times 10^{-2}$	58.3%	0.28	17.4	$1.4 \times 10^{35}$
0.3	0.05	$5.0 \times 10^{-3}$	62.2%	0.22	12.5	$6.6 \times 10^{34}$
0.3	0.05	$1.0 \times 10^{-3}$	62.7%	0.15	10.0	$8.0 \times 10^{33}$
0.3	0.05	$5.0 \times 10^{-4}$	62.7%	0.12	8.90	$2.7 \times 10^{33}$
0.3	0.05	$1.0 \times 10^{-4}$	62.7%	0.082	9.90	$1.4 \times 10^{32}$
0.3	0.05	$5.0 \times 10^{-5}$	62.7%	0.069	13.6	$3.1 \times 10^{31}$
0.3	0.05	$2.0 \times 10^{-5}$	62.7%	0.055	23.1	$3.1 \times 10^{30}$
0.3	0.01	$1.5 \times 10^{-2}$	60.7%	0.19	47.7	$5.5 \times 10^{34}$
0.3	0.01	$5.0 \times 10^{-3}$	62.4%	0.15	39.2	$1.2 \times 10^{34}$
0.3	0.01	$1.0 \times 10^{-3}$	62.7%	0.098	40.5	$8.8 \times 10^{32}$
0.3	0.01	$5.0 \times 10^{-4}$	62.7%	0.082	45.0	$2.4 \times 10^{32}$
0.3	0.01	$2.0 \times 10^{-4}$	62.7%	0.065	56.4	$3.6 \times 10^{31}$
0.3	0.01	$1.0 \times 10^{-4}$	62.7%	0.055	71.6	$8.2 \times 10^{30}$

netic energy of the ADAF, i.e.,  $L'_* \gg L_{\text{bl}}$ . Since the effect of  $\nu_{\text{NS}}$  on the structure of the ADAF is very little, we expect that the effect of  $\nu_{\text{NS}}$  on the corresponding emergent spectrum is also very little, and can be neglected. Here, we should keep in mind that in the present paper, we do not take into account the effect of general relativity for the different value of  $\nu_{\text{NS}}$  on the structure and the corresponding emergent spectrum of the ADAF, which is beyond the scope of the present paper, and will be studied in the future work.

#### 4.2 On the physical origin of the X-ray emission in the quiescent state

In this paper, we theoretically investigate the relation of  $\eta$  versus  $L_{0.5-10\text{keV}}$  in low-level accreting NSs ( $L_{0.5-10\text{keV}} \lesssim 10^{36}$  erg s $^{-1}$ ) within the framework of the self-similar solution of the ADAF around a weakly magnetized NS, in which the thermal soft X-ray component is from the surface of the NS, and the power-law component is from the ADAF itself. However, we would like to mention that when NS-LMXBs are in the quiescent state, i.e.,  $L_{0.5-10\text{keV}} \lesssim 10^{34}$  erg s $^{-1}$ , the origin of both the thermal soft X-ray component and the power-law component of the X-ray spectrum are still under debate (e.g. [Wijnands et al. 2017](#), for review). Observationally, when NS-LMXBs go into the quiescent state, the X-ray spectra are diverse, and three possible X-ray spectra have been observed for different sources. The X-ray spectra can be, (1) totally dominated by the thermal soft X-ray component [hereafter spectrum (1)], or (2) totally dominated by the power-law component [hereafter spec-

trum (2)], or (3) described by the two-component model with a thermal soft X-ray component plus a power-law component [hereafter spectrum (3)]. The spectrum (1) could be produced by the emission of the crust cooling of the NS, which is heated during the outburst (e.g. [Brown et al. 1998](#); [Campana et al. 2000](#); [Rutledge et al. 1999, 2001a,b](#)), and also could be produced by the very low accretion on the surface of the NS, e.g., as the paper of [Qiao & Liu \(2018\)](#), or the present paper with an extreme value of  $f_{\text{th}} = 1$  taken. Currently, the origin of the spectrum (2) is still unclear. It has been proposed that such a spectrum might be related to the magnetic field of the NS as a pulsar-wind mechanism, such as the study of SAX J1808.4-3658 (e.g. [Stella et al. 1994](#); [Burderi et al. 2003](#); [Campana et al. 2002](#)). For the spectrum (3), the thermal soft X-ray component is possible to be produced by the crust cooling of the NS. Meanwhile, the study of the variability property of the thermal soft X-ray component indicates that the origin of the thermal soft X-ray component is more likely due to the low-level accretion onto the surface of the NS, such as the study of Cen X-4 ([Campana et al. 1997, 2004](#); [Cackett et al. 2010, 2013](#)), and Aql X-1 ([Rutledge et al. 2002](#); [Cackett et al. 2011](#); [Bernardini et al. 2013](#)). The origin of the power-law component in the spectrum (3) is unclear, and is also very possible to be related with the low-level accretion onto the surface of the NS ([Zampieri et al. 1995](#); [D'Angelo et al. 2015](#); [Chakrabarty et al. 2014](#)). By fitting the quiescent spectrum of Cen X-4 ( $L_{0.5-10\text{keV}} \sim 10^{33}$  erg s $^{-1}$ ) with the joint *XMM-Newton* and *Nuclear Spectroscopic Telescope Array (NuSTAR)* observations, it is suggested that both the thermal soft X-ray component and the

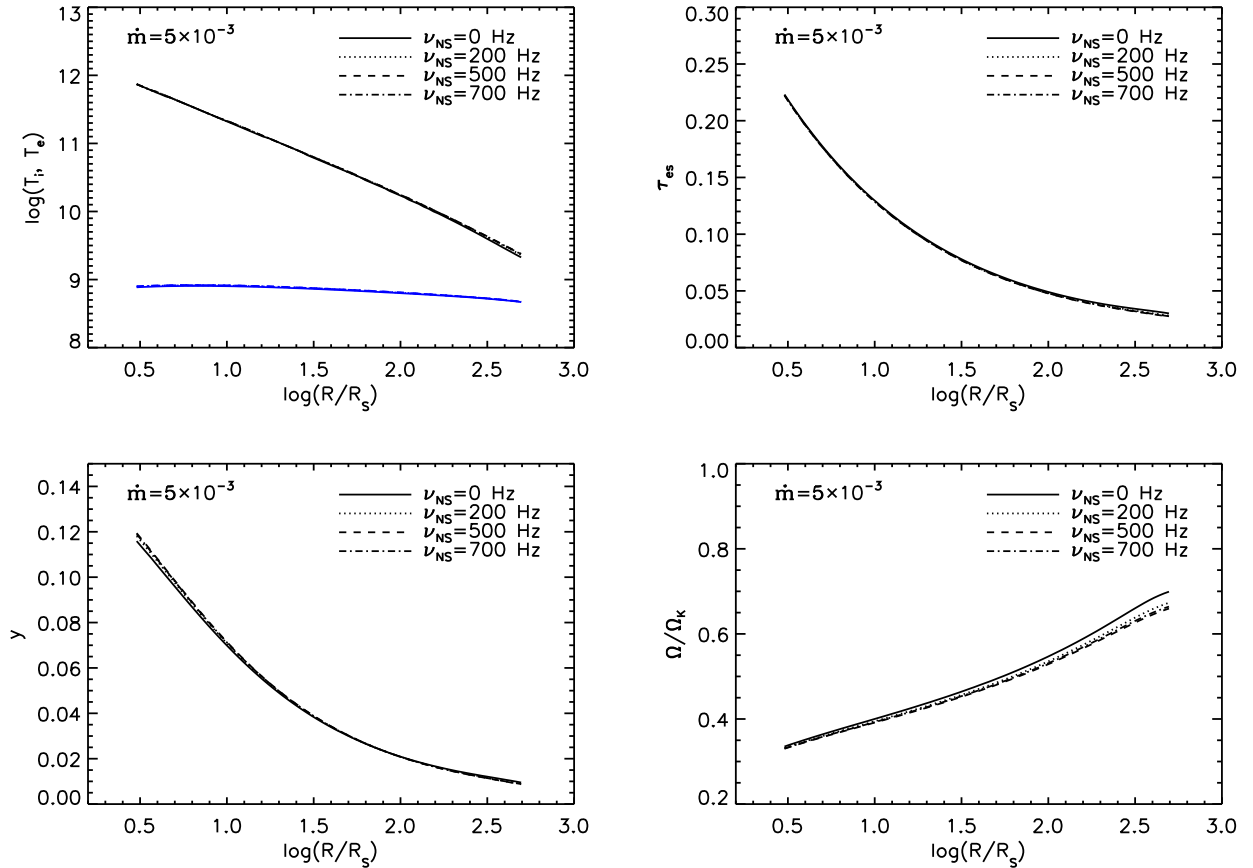


**Figure 8.** Panel (1): Ion temperature  $T_i$  (black line) and electron temperature  $T_e$  (blue line) as a function of radius  $R/R_S$  around NSs for different rotational frequency of the NS  $\nu_{NS}$  with  $\dot{m} = 5 \times 10^{-3}$ . Panel (2): Compton scattering optical depth  $\tau_{es}$  as a function of radius  $R/R_S$  around NSs for different rotational frequency of the NS  $\nu_{NS}$  with  $\dot{m} = 5 \times 10^{-3}$ . Panel (3): Compton  $y$ -parameter as a function of radius  $R/R_S$  around NSs for different rotational frequency of the NS  $\nu_{NS}$  with  $\dot{m} = 5 \times 10^{-3}$ . Panel (4):  $\Omega/\Omega_K$  as a function of radius  $R/R_S$  around NSs for different rotational frequency of the NS  $\nu_{NS}$  with  $\dot{m} = 5 \times 10^{-3}$ . In the calculation, we fix  $\alpha = 0.3$  and  $f_{th} = 1.0$ .

power-law component are due to the low-level accretion onto the surface of the NS (D’Angelo et al. 2015). Specifically, the authors fitted the thermal soft X-ray component with the `NSATMOS` NS atmosphere model (Heinke et al. 2006), and found that the power-law component ( $\Gamma \sim 1 - 1.5$ ) with a cut-off energy  $\sim 10$  keV can be well fitted by the bremsstrahlung from the boundary layer between the surface of the NS and the accretion flow (with the accretion flow here being the radiatively inefficient accretion flow—RIAF). In D’Angelo et al. (2015), the authors argued that the power-law emission comes from the boundary layer rather than the accretion flow itself, so the accretion flow as its name is ‘radiatively inefficient’. One can refer to Section 4.3 on this point for discussions. In a word, we think that the origin of the X-ray emission in the quiescent state of NS-LMXBs is very complicated, the understanding to which depends on both the strict theoretical and observational investigations in the future.

### 4.3 The radiative efficiency of NSs with an ADAF accretion

The defining property of ADAF as its name ‘advection-dominated accretion flow’, is that a large fraction of the viscously dissipated energy will be stored in the accretion flow and advected onto the central compact object (BH or NS) rather than be directly radi-

ated out in the accretion flow itself. In BH case, the advected energy will ‘vanish’ as passing through the event horizon of the BH. While in NS case, it is often suggested that such energy advected onto the surface of the NS will eventually be radiated out (Narayan & McClintock 2008, for review). As we can see in Section 3.1, the energy of the ADAF transferred onto the surface of the NS (including the internal energy, the radial kinetic energy and the rotational energy) is dependent on the viscosity parameter  $\alpha$ , i.e.,  $L_*/L_G$  increases with increasing  $\alpha$ . The value of  $L_*/L_G$  is in the range of  $\sim 60 - 80\%$  for different  $\alpha$ , which is higher than of the thin disc of  $L_*/L_G = 50\%$  in the framework of the Newtonian mechanics. For the thin disc around a NS, half of the gravitational energy will be released in the accretion disc as,

$$L_d = \frac{1}{2} \dot{M} \frac{GM}{R_*}, \quad (6)$$

and the energy transferred onto the surface of the NS (or released in the boundary layer between the disc and the NS) can be seen as in equation 2, and can be further re-expressed as,

$$L_{bl} = \frac{1}{2} \dot{M} k \frac{GM}{R_*} \left( 1 - \frac{\nu_{NS}}{v_*} \right)^2, \quad (7)$$

where  $k=1$ . The total radiative luminosity of the NS accreting system is  $L_{rad} = L_d + L_{bl}$ . If  $\nu_{NS} = 0$ ,  $L_d$  is equal to  $L_{bl}$ , and the rad-

diative efficiency of the NS accreting system is  $\epsilon = L_{\text{rad}}/\dot{M}c^2 = L_{\text{d}}/\dot{M}c^2 + L_{\text{bl}}/\dot{M}c^2 \sim 0.1 + 0.1 = 0.2$ .

For the ADAF around a NS, if the energy transferred onto the surface of the NS can be eventually radiated out, i.e. taking  $f_{\text{th}} = 1$  in our model, the total radiative luminosity is  $L_{\text{rad}} = L_{\text{ADAF}} + L_* = \dot{M}\frac{GM}{R_*}$ , and the radiative efficiency of the NS accreting system is  $\epsilon = L_{\text{rad}}/\dot{M}c^2 \sim 0.2$ . However, as can be seen in Section 3.2, in order to match the observed range of the fractional contribution of the power-law luminosity  $\eta$  and the relation of  $\eta$  versus  $L_{0.5-10\text{keV}}$ , it implies that  $f_{\text{th}}$  is at least less than 0.1. For example, if we take  $\alpha = 0.3$  and  $f_{\text{th}} = 0.1$ , the total radiative luminosity is  $L_{\text{rad}} = L_{\text{ADAF}} + f_{\text{th}}L_* = L_{\text{ADAF}} + 0.1L_* \sim (100\% - 60\%)\dot{M}\frac{GM}{R_*} + 0.1 * 60\% * \dot{M}\frac{GM}{R_*} = 0.46\dot{M}\frac{GM}{R_*}$ , and the radiative efficiency is  $\epsilon = L_{\text{rad}}/\dot{M}c^2 \sim 0.46 \times 2 \times 0.1 \sim 0.09$ . For  $\alpha = 0.3$  and  $f_{\text{th}} = 0.01$ , the result is similar, and the radiative efficiency is  $\epsilon = L_{\text{rad}}/\dot{M}c^2 \sim 0.406 \times 2 \times 0.1 \sim 0.08$ . Here we should note that, although the radiative efficiency of the NS may not be as high as the predicted results previously of  $\epsilon \sim \frac{MG\dot{M}}{R_*\dot{M}c^2} \sim 0.2$ , the radiative efficiency of the NS with an ADAF accretion is still significantly higher than that of the BH. The radiative efficiency of the NS with an ADAF accretion nearly does not depend on  $\dot{m}$  with  $\epsilon$  always  $\sim 0.08 - 0.09$ . The radiative efficiency of the BH with an ADAF accretion is completely different, which is very dependent on  $\dot{m}$ . If  $\dot{m}$  is approaching the critical mass accretion rate of  $\dot{M}'_{\text{crit}} \sim \alpha^2 \dot{M}_{\text{Edd}}$ , the radiative efficiency is approaching the value of the thin disc as  $\epsilon \sim 0.1$ , while  $\epsilon$  dramatically decreases with decreasing  $\dot{m}$  with a form of  $\epsilon \propto \dot{m}^a$ . Specifically,  $a$  is 0.71 for  $\dot{m} \lesssim 7.6 \times 10^{-5}$ ,  $a$  is 0.47 for  $7.6 \times 10^{-5} \lesssim \dot{m} \lesssim 4.5 \times 10^{-3}$ , and  $a$  is 3.67 for  $4.5 \times 10^{-3} \lesssim \dot{m} \lesssim 7.1 \times 10^{-3}$  (with the parameter of direct heating to the electrons  $\delta = 10^{-3}$  assumed). For example,  $\epsilon \sim 8\%$ ,  $\sim 0.6\%$ ,  $\sim 0.2\%$  and  $\sim 0.04\%$  for  $\dot{m} = 10^{-2}$ ,  $10^{-3}$ ,  $10^{-4}$  and  $10^{-5}$  respectively (Xie & Yuan 2012).

In this paper, we assume that only a fraction,  $f_{\text{th}}$ , of the total energy of the ADAF transferred onto the surface of the NS is thermalized at the surface of the NS as the soft photons to be scattered in the ADAF itself, which means that the remaining fraction,  $1 - f_{\text{th}}$ , of the total energy of the ADAF transferred onto the surface of the NS is not radiated out. One of the possibilities is that such a fraction of the energy is converted to the rotational energy of the NS, making the rotational frequency  $\nu_{\text{NS}}$  of the NS increased. For example, if we take  $\alpha = 0.3$  and  $f_{\text{th}} = 0.1$ , the energy converted to the rotational energy of the NS per second is  $\dot{E} = (1 - f_{\text{th}})L_* = (1 - 0.1) * 60\% * \dot{M}\frac{GM}{R_*} \sim 0.5\dot{M}\frac{GM}{R_*}$ . For a typical value of  $M = 1.4M_{\odot}$ ,  $R_* = 12.5$  km, and  $\dot{M} = 10^{-3}\dot{M}_{\text{Edd}}$ ,  $\dot{E} \sim 1.76 \times 10^{35}$  erg s $^{-1}$ . As we know, the rotational kinetic energy of the NS can be expressed as,

$$E = \frac{1}{2}I\Omega_{\text{NS}}^2, \quad (8)$$

where  $I$  is the moment of inertia, and  $\Omega_{\text{NS}}$  (with  $\Omega_{\text{NS}} = 2\pi\nu_{\text{NS}}$ ) is the rotational angular velocity of the NS. For a typical value of  $M = 1.4M_{\odot}$ , and  $R_* = 12.5$  km,  $I \sim 1.75 \times 10^{45}$  g cm $^2$ . Assuming  $\nu_{\text{NS}} = 500$  Hz,  $E \sim 8.7 \times 10^{51}$  erg. Roughly, the time scale for the rotational frequency of the NS increases from  $\nu_{\text{NS}} = 0$  to  $\nu_{\text{NS}} = 500$  is  $t \sim E/\dot{E} \sim 1.6 \times 10^9$  years. So a significant change of the rotational frequency in the range of our observable time is very little, and nearly can be neglected. Meanwhile, more importantly, as discussed in Section 4.1, the effect of the NS spin on the structure and corresponding emergent spectrum is very little, so our assumption in this paper is self-consistent. We should also keep in mind, in the present paper, all our conclusions are based on the self-similar solution of the ADAF around a weakly magnetized NS. Especially, we are not clear whether the structure and the radiative property of

the ADAF can significantly change or not for different  $\nu_{\text{NS}}$  if the global solution of the ADAF around a NS is considered, which is very important and will be studied in the future work.

Here we would like to mention an interesting paper of D'Angelo et al. (2015). As has been discussed in Section 4.2, by fitting the broad band quiescent X-ray spectrum of Cen X-4, D'Angelo et al. (2015) concluded that the power-law component of the X-ray spectrum is from the boundary layer between the surface of the NS and the accretion flow rather than the accretion flow itself, and further concluded that the accretion flow is 'radiatively inefficient' as similar as Chakrabarty et al. (2014). However, as far as the viewing point of the energy balance, in D'Angelo et al. (2015), although the accretion flow is 'radiatively inefficient', most of the energy released in the accretion process is radiated out in the boundary layer, the whole accreting system itself is still radiatively efficient. Actually, the radiative efficiency from D'Angelo et al. (2015) is not deviated from that of our model. Furthermore, we would like to point out that the fraction of the accretion energy released in the boundary layer or the accretion flow itself is uncertain, which can be affected by several factors, such as the spin and the magnetic field of the NS. A more detailed study of the low-level accretion onto NSs by considering the spin and the magnetic field of the NS is still necessary in the future work.

## 5 CONCLUSIONS

In this paper, we systematically investigate the X-ray emission in weakly magnetized low-level accreting NSs within the framework of the self-similar solution of the ADAF as in Qiao & Liu (2018), in which the soft X-ray emission is from the surface of the NS and the power-law X-ray emission is from the ADAF itself respectively. Additionally, in this paper, we update the calculation of Qiao & Liu (2018) with the effect of the NS spin considered. We test the effect of the viscosity parameter  $\alpha$  and the thermalized parameter  $f_{\text{th}}$  on the relation between the fractional contribution of the power-law luminosity  $\eta$  and the X-ray luminosity  $L_{0.5-10\text{keV}}$ . It is found that the effect of  $\alpha$  on the relation between  $\eta$  and  $L_{0.5-10\text{keV}}$  is very little, and nearly can be neglected, while the effect of  $f_{\text{th}}$  on the relation between  $\eta$  and  $L_{0.5-10\text{keV}}$  is very significant. By comparing with a sample of non-pulsating NS-LMXBs probably dominated by low-level accretion onto NSs, it is found that a small value of  $f_{\text{th}} \lesssim 0.1$  is needed to match the observed range of  $\eta \gtrsim 10\%$  in the diagram of  $\eta$  versus  $L_{0.5-10\text{keV}}$ . We argue that the small value of  $f_{\text{th}} \lesssim 0.1$  implies that only a small fraction of the energy transferred onto the surface of the NS can be radiated out for the ADAF around a NS. Meanwhile, we think that it is very possible that the remaining fraction,  $1 - f_{\text{th}}$ , of the energy transferred onto the surface of the NS can be converted to the rotational kinetic energy of the NS. So the radiative efficiency of a weakly magnetized NS with an ADAF accretion may not be as higher as the predicted results previously of  $\epsilon \sim 0.2$  despite the existence of the hard surface. Here we would like to mention that although a great of efforts have been made for investigating the X-ray spectrum of NS-LMXBs as in the low-level accretion regime, the detailed physical mechanism for the interaction between the accretion flow and the NS is still under debate (e.g. Wijnands et al. 2015, for discussions). Finally, our model intrinsically predicts a positive correlation between  $\eta$  and  $L_{0.5-10\text{keV}}$  for  $L_{0.5-10\text{keV}} \gtrsim$  a few times of  $10^{33}$  erg s $^{-1}$ , and an anti-correlation between  $\eta$  and  $L_{0.5-10\text{keV}}$  for  $L_{0.5-10\text{keV}} \lesssim$  a few times of  $10^{33}$  erg s $^{-1}$  for taking  $f_{\text{th}} = 0.1, 0.05$  and  $0.01$  respectively, which we expect can be confirmed by more accurate observations in the future.



## ACKNOWLEDGMENTS

This work is supported by the National Natural Science Foundation of China (Grants 11773037 and 11673026), the gravitational wave pilot B (Grants No. XDB23040100), the Strategic Pioneer Program on Space Science, Chinese Academy of Sciences (Grant No. XDA15052100) and the National Program on Key Research and Development Project (Grant No. 2016YFA0400804).

## REFERENCES

- Allen J. L., Homan J., Chakrabarty D., Nowak M., 2018, *ApJ*, **854**, 58
- Armas Padilla M., Degenaar N., Wijnands R., 2013a, *MNRAS*, **434**, 1586
- Armas Padilla M., Wijnands R., Degenaar N., 2013b, *MNRAS*, **436**, L89
- Asai K., Dotani T., Mitsuda K., Hoshi R., Vaughan B., Tanaka Y., Inoue H., 1996, *PASJ*, **48**, 257
- Bahramian A., et al., 2014, *ApJ*, **780**, 127
- Bernardini F., Cackett E. M., Brown E. F., D'Angelo C., Degenaar N., Miller J. M., Reynolds M., Wijnands R., 2013, *MNRAS*, **436**, 2465
- Brown E. F., Bildsten L., Rutledge R. E., 1998, *ApJ*, **504**, L95
- Bu D.-F., Qiao E., Yang X.-H., 2019, *ApJ*, **875**, 147
- Burderi L., Di Salvo T., D'Antona F., Robba N. R., Testa V., 2003, *A&A*, **404**, L43
- Cackett E. M., Brown E. F., Miller J. M., Wijnands R., 2010, *ApJ*, **720**, 1325
- Cackett E. M., Fridriksson J. K., Homan J., Miller J. M., Wijnands R., 2011, *MNRAS*, **414**, 3006
- Cackett E. M., Brown E. F., Degenaar N., Miller J. M., Reynolds M., Wijnands R., 2013, *MNRAS*, **433**, 1362
- Campana S., Mereghetti S., Stella L., Colpi M., 1997, *A&A*, **324**, 941
- Campana S., Colpi M., Mereghetti S., Stella L., Tavani M., 1998, *A&ARv*, **8**, 279
- Campana S., Stella L., Mereghetti S., Cremonesi D., 2000, *A&A*, **358**, 583
- Campana S., et al., 2002, *ApJ*, **575**, L15
- Campana S., Israel G. L., Stella L., Gastaldello F., Mereghetti S., 2004, *ApJ*, **601**, 474
- Campana S., Stella L., Kennea J. A., 2008a, *ApJ*, **684**, L99
- Campana S., Stella L., Israel G., D'Avanzo P., 2008b, *ApJ*, **689**, L129
- Campana S., Brivio F., Degenaar N., Mereghetti S., Wijnands R., D'Avanzo P., Israel G. L., Stella L., 2014, *MNRAS*, **441**, 1984
- Casella P., Altamirano D., Patruno A., Wijnands R., van der Klis M., 2008, *ApJ*, **674**, L41
- Chakrabarty D., et al., 2014, *ApJ*, **797**, 92
- D'Angelo C. R., Fridriksson J. K., Messenger C., Patruno A., 2015, *MNRAS*, **449**, 2803
- Degenaar N., Suleimanov V. F., 2018, Testing the Equation of State with Electromagnetic Observations. p. 185, doi:10.1007/978-3-319-97616-7\_5
- Degenaar N., et al., 2009, *MNRAS*, **396**, L26
- Degenaar N., Wijnands R., Miller J. M., 2013, *ApJ*, **767**, L31
- Done C., Gierliński M., 2003, *MNRAS*, **342**, 1041
- Esin A. A., McClintock J. E., Narayan R., 1997, *ApJ*, **489**, 865
- Frank J., King A., Raine D. J., 2002, *Accretion Power in Astrophysics: Third Edition*
- Fridriksson J. K., et al., 2010, *ApJ*, **714**, 270
- Fridriksson J. K., et al., 2011, *ApJ*, **736**, 162
- Gilfanov M. R., Sunyaev R. A., 2014, *Physics Uspekhi*, **57**, 377
- Hasinger G., van der Klis M., 1989, *A&A*, **225**, 79
- Heinke C. O., Rybicki G. B., Narayan R., Grindlay J. E., 2006, *ApJ*, **644**, 1090
- Heinke C. O., Jonker P. G., Wijnands R., Taam R. E., 2007, *ApJ*, **660**, 1424
- Heinke C. O., Jonker P. G., Wijnands R., Deloye C. J., Taam R. E., 2009, *ApJ*, **691**, 1035
- Homan J., Fridriksson J. K., Wijnands R., Cackett E. M., Degenaar N., Linares M., Lin D., Remillard R. A., 2014, *ApJ*, **795**, 131
- Inogamov N. A., Sunyaev R. A., 1999, *Astronomy Letters*, **25**, 269
- Jonker P. G., Wijnands R., van der Klis M., 2004a, *MNRAS*, **349**, 94
- Jonker P. G., Galloway D. K., McClintock J. E., Buxton M., Garcia M., Murray S., 2004b, *MNRAS*, **354**, 666
- Liu B. F., Yuan W., Meyer F., Meyer-Hofmeister E., Xie G. Z., 1999, *ApJ*, **527**, L17
- Mahadevan R., 1997, *ApJ*, **477**, 585
- Manmoto T., Mineshige S., Kusunose M., 1997, *ApJ*, **489**, 791
- Medvedev M. V., 2004, *ApJ*, **613**, 506
- Medvedev M. V., Narayan R., 2001, *ApJ*, **554**, 1255
- Meyer F., Liu B. F., Meyer-Hofmeister E., 2000a, *A&A*, **354**, L67
- Meyer F., Liu B. F., Meyer-Hofmeister E., 2000b, *A&A*, **361**, 175
- Narayan R., McClintock J. E., 2008, *New Astron. Rev.*, **51**, 733
- Narayan R., Yi I., 1995, *ApJ*, **452**, 710
- Nowak M. A., Wilms J., Dove J. B., 2002, *MNRAS*, **332**, 856
- Parikh A. S., Wijnands R., Degenaar N., Altamirano D., Patruno A., Gusinskaia N. V., Hessels J. W. T., 2017, *MNRAS*, **468**, 3979
- Popham R., Narayan R., 1992, *ApJ*, **394**, 255
- Popham R., Sunyaev R., 2001, *ApJ*, **547**, 355
- Qiao E., Liu B. F., 2009, *PASJ*, **61**, 403
- Qiao E., Liu B. F., 2010, *PASJ*, **62**, 661
- Qiao E., Liu B. F., 2013, *ApJ*, **764**, 2
- Qiao E., Liu B. F., 2018, *MNRAS*, **481**, 938
- Qiao E., Liu B. F., 2019, *MNRAS*, **487**, 1626
- Qiao E., Liu B. F., Panessa F., Liu J. Y., 2013, *ApJ*, **777**, 102
- Rivera Sandoval L. E., et al., 2018, *MNRAS*, **479**, 2777
- Rutledge R. E., Bildsten L., Brown E. F., Pavlov G. G., Zavlin V. E., 1999, *ApJ*, **514**, 945
- Rutledge R. E., Bildsten L., Brown E. F., Pavlov G. G., Zavlin V. E., 2000, *ApJ*, **529**, 985
- Rutledge R. E., Bildsten L., Brown E. F., Pavlov G. G., Zavlin V. E., 2001a, *ApJ*, **551**, 921
- Rutledge R. E., Bildsten L., Brown E. F., Pavlov G. G., Zavlin V. E., 2001b, *ApJ*, **559**, 1054
- Rutledge R. E., Bildsten L., Brown E. F., Pavlov G. G., Zavlin V. E., 2002, *ApJ*, **577**, 346
- Shakura N. I., Sunyaev R. A., 1973, *A&A*, **24**, 337
- Sibgatullin N. R., Sunyaev R. A., 2000, *Astronomy Letters*, **26**, 699
- Stella L., Campana S., Colpi M., Mereghetti S., Tavani M., 1994, *ApJ*, **423**, L47
- Sunyaev R. A., Shakura N. I., 1986, *Soviet Astronomy Letters*, **12**, 117
- Taam R. E., Liu B. F., Yuan W., Qiao E., 2012, *ApJ*, **759**, 65
- Tomsick J. A., Gelino D. M., Halpern J. P., Kaaret P., 2004, *ApJ*, **610**, 933
- Vats S., Wijnands R., Parikh A. S., Ootes L., Degenaar N., Page D., 2018, *MNRAS*, **477**, 2494
- Wijnands R., Miller J. M., Markwardt C., Lewin W. H. G., van der Klis M., 2001, *ApJ*, **560**, L159
- Wijnands R., Homan J., Miller J. M., Lewin W. H. G., 2004, *ApJ*, **606**, L61
- Wijnands R., Heinke C. O., Pooley D., Edmonds P. D., Lewin W. H. G., Grindlay J. E., Jonker P. G., Miller J. M., 2005, *ApJ*, **618**, 883
- Wijnands R., Degenaar N., Armas Padilla M., Altamirano D., Cavecchi Y., Linares M., Bahramian A., Heinke C. O., 2015, *MNRAS*, **454**, 1371
- Wijnands R., Degenaar N., Page D., 2017, *Journal of Astrophysics and Astronomy*, **38**, 49
- Xie F.-G., Yuan F., 2012, *MNRAS*, **427**, 1580
- Yuan F., Narayan R., 2014, *ARA&A*, **52**, 529
- Zampieri L., Turolla R., Zane S., Treves A., 1995, *ApJ*, **439**, 849
- Zhang G., Méndez M., Jonker P., Hiemstra B., 2011, *MNRAS*, **414**, 1077

This paper has been typeset from a  $\text{\TeX}/\text{\LaTeX}$  file prepared by the author.